Lawrence Berkeley National Laboratory
Recent Work

Title

Experiments and Modeling of the Soil-Gas Transport of Volatile Organic Compounds into a Residential Basement

Permalink

https://escholarship.org/uc/item/1xm7p52k

Author

Garbesi, K.

Publication Date

1988-07-01

eScholarship.org Powered by the California Digital Library
University of California

UC 402
LBL-25519 c.1

Lawrence Berkeley Laboratory
UNIVERSITY OF CALIFORNIA

APPLIED SCIENCE DIVISION

Experiments and Modeling of the Soil-Gas Transport of Volatile Organic Compounds into a Residential Basement

K. Garbesi
(M.S. Thesis)

LAWRENCE
OCT 1988
ENTS SEC

July 1988

For Reference

Not to be taken from this room

APPLIED SCIENCE DIVISION

LBL-25519 c.1

Prepared for the U.S. Department of Energy under Contract Number DE-AC03-76SF00098.

DISCLAIMER

This document was prepared as an account of work sponsored by the United States Government. While this document is believed to contain correct information, neither the United States Government nor any agency thereof, nor the Regents of the University of California, nor any of their employees, makes any warranty, express or implied, or assumes any legal responsibility for the accuracy, completeness, or usefulness of any information, apparatus, product, or process disclosed, or represents that its use would not infringe privately owned rights. Reference herein to any specific commercial product, process, or service by its trade name, trademark, manufacturer, or otherwise, does not necessarily constitute or imply its endorsement, recommendation, or favoring by the United States Government or any agency thereof, or the Regents of the University of California. The views and opinions of authors expressed herein do not necessarily state or reflect those of the United States Government or any agency thereof or the Regents of the University of California.

LBL-25519

EXPERIMENTS AND MODELING OF THE SOIL-GAS TRANSPORT OF VOLATILE ORGANIC COMPOUNDS INTO A RESIDENTIAL BASEMENT

by Karina Garbesi

A thesis submitted in partial fulfillment
of the requirements for the degree of
Master of Science
(Energy and Resources)
University of California, Berkeley
1988

Indoor Environment Program
Lawrence Berkeley Laboratory
University of California
Berkeley, CA 94720

This work was funded by the Occidental Chemical Corporation, through Agreement BG-8602A with the United States Department of Energy. It was supported by the Assisstant Secretary for Conservation and Renewable Energy , Office of Building and Community Systems, Building Systems Division, and by the Director, Office of Energy Research, Office of Health and Environmental Research, Human Health Assessments Division, and Pollutant Characterization and Safety Research Division of the U.S. Department of Energy under Contract No. DE-ACO3-76SF00098.

to Marc

TABLE OF CONTENTS

List of Figures and Tables

ABSTRACT

In the past it was assumed that the major pathway for migration of contaminants from landfills was through contamination and movement of groundwater. Recently, the discovery of the migration of methane gas from landfills into nearby residences has indicated the importance of gas-phase transport. Research on the entry of radon gas into houses indicates that the pressure-driven entry of soil gas can result in high indoor concentrations of soil-gas contaminants. This paper presents theoretical and laboratory studies of the advective flow of volatile organics compounds (VOC) through soil, and a field investigation of the pressure-driven entry of VOC into a house adjacent to a municipal landfill. The principals of fluid mechanics are used to derive an analytical model of the pressure-driven flow of VOC in soil. The calculation results in the definition of a retardation factor of VOC with respect to the velocity of the bulk soil gas. The retardation equation is then tested in soil-column experiments using sulfur hexafluoride (SF_6) and hexafluorobenzene (HFB). The measured retardation is in good agreement with the predicted value. These experiments are used to evaluate the potential of SF_6 and HFB as tracer gases for use in a field investigation of the advective flow of soil gas into and near the basement of a house near a landfill and to evaluate the potential of the soil-column apparatus for use in screening the advective mobility of VOC important as landfill gas contaminants. The field study consisted of experiments investigating the influence of basement depressurization on the surrounding soil gas, and quantifying VOC contamination at the site. Soil-gas entry into the house during artificial basement depressurization was measured using SF_6 as a tracer, and pressure coupling was measured between the basement and the surrounding soil. Measurements of VOC in ambient air, indoor air, and soil gas indicate that a number of halogenated and oxygenated contaminants present in indoor air had a soil-gas source. Particularly high concentrations of dichlorodifluoromethane, trichlorofluoromethane, and tetrachloroethylene were identified in the soil gas. The pressure field generated in the soil around the basement by basement underpressure was modeled using a modified groundwater model. The advantage of this model over previous models used for this purpose is the flexibility offered to the user to assign different permeabilities to different elements representing the soil and building shell. This feature allowed the model to be used easily for site specific analysis, and to determine the effect of soil layering and basement leakage geometry on the pressure-field.

ACKNOWLEDGMENTS

My Master's Thesis research was part of a collaboration between the Organics and Radon Groups of the Indoor Environment Program at Lawrence Berkeley Laboratory (LBL). During the course of my research I worked closely with both groups. I was fortunate to have joined the Radon Group at the outset of the project and, therefore, to have been involved in the project direction at every stage.

I would like to acknowledge the help and support I received from many people on my Master's research. I first want to thank my thesis advisor, Dr. Richard Sextro. The original conception of the project was his and he worked closely with me in every stage of the work. Without his generous and abundant help in the laboratory and the field and without the many long discussions over data interpretation and theory, I would not have been able to complete this project. I am especially grateful for his partnership during many long and arduous hours in the field.

Another continuous partner in my work was Al Hodgson, staff scientist in the Organics Group at LBL. During the course of the project he has taught me a great deal about laboratory techniques and equipment, conducting field work, and writing scientific reports. Mr. Hodgson was the principal author of Chapter 4 of this paper. That Chapter was written and accepted as a paper for presentation to the 81st annual meeting of the Air Pollution Control Association (Hodgson *et al.*, 1988). The research presented in the chapter was divided in the following manner. Mr. Hodgson was primarily responsible for the VOC experiments and I was primarily responsible for the experiments investigating the physical mechanisms of soil gas flow and pressure coupling. I want to thank him especially for his careful editing of the entire paper, which has led to many significant improvements.

Ken Revzan pointed the way for the derivation of the equation in Appendix A for soil permeability to air as determined by in-situ permeability measurements. My sincere thanks

also to other members of both the Radon and Organics groups, especially to Dr. Joan Daisey for her encouragement and to Brad Turk and Rich Prill for help with laboratory equipment and computers. I want to acknowledge Professor Nicholaus Sitar of Civil Engineering at the University of California, Berkeley, for the use of his groundwater model which formed the basis of the analysis of Chapter 5 of this paper. I thank Professor Harvey Donner and Scott Rogers for teaching me the soil organic carbon analysis technique and Dr. Rudy Glauser for the use of his laboratory for the soil particle-size distribution analysis. I also acknowledge Prof. Mark Christensen of the Energy and Resources Group (ERG) at UC Berkeley as the ERG reader of my Master's Thesis. Special thanks also to the owners of the house at which the field study was conducted for making it available for research.

CHAPTER 1

STUDY OBJECTIVES AND ORGANIZATION

Introduction

Until recently it was assumed that contamination of groundwater was the only important potential pathway for the migration of pollutants from landfills. The discovery of the migration of methane gas from landfills brought this assumption into question. At one hazardous waste disposal site methane and trace contaminants of the landfill gas were found migrating off-site and into adjacent homes. Methane concentrations measured under sinks in these houses neared one percent (Wood and Porter, 1987). A study by the State of California demonstrating that essentially all landfills produce methane (CWMB, 1985) is an indication that even nonhazardous landfills could present a public health risk. In 1984 the California Legislature acknowledged the potential threat by passing a law requiring the testing of landfill gas at all nonhazardous solid waste disposal sites for composition and off-site migration (California Health and Safety Code, Section 41805.5, 1986). The data from this testing program are scheduled for summary and review by the Legislature in 1989.

A study by Wood and Porter (1987) of 20 municipal landfills indicate that even municipal landfills, authorized to accept only nonhazardous material, contain toxic volatile organic compounds (VOC) at elevated concentrations. In their study, the authors found vinyl chloride and benzene at detectable levels in the landfill gas of 85 percent of the sites, often at concentrations exceeding 1 ppm. Several landfills closed for many years were among those with elevated concentrations of these compounds. Detailed investigation at one site revealed gas-phase migration of toxic trace-contaminants off site with low boiling point compounds traveling farthest through the soil. The authors concluded that there is a potential for indoor exposure due to subsurface landfill gas migration at a large percentage of sites.

The entry of soil gas into houses has been studied in relation to the issue of indoor radon.

It has been demonstrated that advective flow of soil gas into substructures is the primary source of radon gas in single-family residences with elevated concentrations (Nero and Nazaroff, 1984; Sextro *et al.*, 1987). This flow is driven by depressurization of the substructure with respect to the surrounding soil. Depressurization of a few Pascals results from the stack effect caused by thermal differences between indoors and outdoors and from the Bernoulli effect from wind loading on the building superstructure (Nazaroff *et al*, 1985 and Nazaroff *et al*, 1987). If the soil is sufficiently permeable, a persistent pressure differential can draw soil-gas bearing contaminants into a house at a higher rate than would be predicted by diffusion alone. In one field study, pressure coupling between basements and surrounding soil was measured, and the entry of soil gas was demonstrated using a tracer-gas technique (Nazaroff *et al*, 1987). While significant differences from radon are expected due to differences in the physical and chemical properties of VOC, it is clear that VOC in soil gas around landfills can enter houses via the same advective-flow pathway.

Because it is likely that volatile trace contaminants present in the landfill gas are transported under the influence of the pressure gradient resulting from the generation of methane within the landfill, an estimation of the potential for the long-distance, subsurface transport of VOC requires an understanding of the pressure-driven flow of gas through soil and the behavior of VOC under such conditions. Most research to date on contaminant migration through soils has focused on the aqueous phase. In particular, Bennett (1986) and Roy and Griffin (1987) have pointed out that this is true of studies on the potential movement of organic solvents, an important constituent in landfill gas contamination. In cases where gas-phase migration has been studied, transport by diffusion has been emphasized. Only recently has gas-phase advective flow come under serious scrutiny as a mechanism for contaminant transport in soils, and this study has only considered transport close to buildings which induce a pressure gradient in the surrounding soil (Nazaroff *et al.*, 1987; Sextro *et al.*, 1987) .

The prediction of the migration of gas-phase contaminants in the sub-surface depends on a knowledge of both soil and contaminant characteristics and of transport driving forces. Most

of the relevant soil characteristics, organic carbon content, water content, bulk density, porosity, and clay content (for dry soils) can be determined by standard laboratory methods. Soil permeability, the parameter which determines soil gas flow rate due to a pressure gradient, can be measured in-situ, as described in the Appendix.

Estimates of the chemical parameters which affect VOC transport, such as Henry's Law constant and the soil sorption coefficient, are more difficult to obtain. Although there are some compiled data of Henry's Law constants for VOC of interest (Mackay and Shiu, 1981) few data on soil sorption coefficients exist. Estimates of soil sorption have been made based on water solubility or octanol-water partitioning, but they are based primarily on pesticide data. Since pesticides are generally designed to be immobile on soil, they are probably not a good model for VOC. The result is a large uncertainty in predicted vapor-phase migration of VOC.

The objectives of the present study were to:

1) Investigate the soil and chemical parameters which influence advection, diffusion, and retardation of VOC during gas-phase transport in soil.

2) Develop an experimental apparatus for the investigation of pressure-driven flow of VOC through soil.

3) Test potential tracer-gases for use in field investigations of the pressure-driven flow of soil gas.

4) Establish by direct measurement that pressure-driven flow of soil gas can result in the transport of VOC into houses.

5) Study the physical mechanisms of soil-gas entry into house substructures.

This paper presents the theoretical, laboratory, and field studies used to achieve the goals outlined above. The theory and soil-column experiments of Chapters 2 and 3, respectively,

investigate the soil and chemical parameters which determine advection, diffusion, and retardation of VOC in soil. These studies lay the foundation of an investigation of the potential of long-distance, gas-phase transport of VOC in the subsurface. Using the principals of fluid-mechanics, the one-dimensional advection-diffusion equation is derived for the gas-phase transport of VOC in soil. The derivation results in the definition of a retardation factor which determines the contaminant velocity with respect to the velocity of the bulk soil gas. Using a soil-column apparatus and experimental method developed for the investigation of pressure-driven flow of VOC through soil the predicted retardation factor is tested by comparing the transport of two testgases, sulfur-hexafluoride (SF_6) and hexafluorobenzene (HFB). Further experimentation with these two compounds are used to evaluate the apparatus and method for use in screening the advective mobility of VOC important as landfill gas contaminants. The results of these experiments were used to assess the potential of SF_6 and HFB for use as tracer gases in the field study.

The field study of the entry of VOC via soil gas into a residential basement was conducted at a Central California house located adjacent to a municipal landfill with a history of off-site methane migration. The field study, described in Chapter 4, consisted of an investigation of the influence of basement depressurization on the surrounding soil gas and quantification of VOC contamination at the site. Two phenomena were measured during artificial depressurization of the basement, pressure coupling between the basement and the surrounding soil, and soil-gas entry as a function of depressurization. Soil-gas entry was measured using SF_6 as a soil-gas tracer, and coupling was determined by measuring the pressure in soil probes installed in the lawn out to 12 m from the house. VOC concentrations were quantified for indoor air, outdoor air, and soil gas, using a multisorbent sampling technique and analysis by gas chromatograph and a mass selective detector.

Chapter 5 describes modeling of the pressure field around the house under the experimental conditions of basement depressurization described in Chapter 4. The pressure

field is modeled with various permeability and basement leakage geometries to investigate the influence of these factors on the shape and extent of the pressure field. The various runs of the model are then compared with the field data to determine plausible mechanisms to explain the observed coupling. In Chapter 6 conclusions of the research are presented and recommendations are made for further study.

DISCLAIMER

Although there is reason to believe that VOC measured in the soil gas at the field site originated in the adjacent landfill, no attempt was made to study the long-distance transport of VOC from the landfill to the house. Nor was any evaluation made of the effectiveness of air-injection pumps installed between the landfill and the house to block the migration of methane gas from the fill. Concentrations of VOC in the soil gas at the site may or may not have been altered by the operation of the pumps. Therefore, the concentrations of VOC measured in and around the house are not necessarily representative of exposures to the former occupants, and no attempt was made to estimate potential health hazards to the former occupants based on the exposures estimated in the present study.

CHAPTER 2

THE THEORY OF PRESSURE-DRIVEN TRANSPORT OF GAS-PHASE VOC IN SOIL

INTRODUCTION

The mechanisms of advection, diffusion, and contaminant retardation, as they apply to the migration of volatile organic compounds (VOC) in soil, are described in this chapter. Darcy's Law, which governs pressure-driven advective flow, and Fick's Law of molecular diffusion are outlined. The various soil and chemical factors influencing VOC retention and retardation are discussed. In particular, equilibrium partitioning between the gas, aqueous, and solid phases is discussed. In addition, the distinction between mineral surface adsorption and partitioning into soil organic carbon is clarified.

A one-dimensional, time-dependent advection-diffusion equation for the transport of gas-phase VOC through soils is developed. The equation assumes equilibrium partitioning of VOC between the soil air, water, and solid phases at all points along the transport path. That is, although a concentration gradient might exist along the path, equilibrium partitioning is assumed to apply at each point. Making use of equilibrium partitioning relationships in a complex multi-phase medium like soil significantly simplifies the theoretical analysis of a transport problem. However, the equilibrium assumption may not always be valid and due consideration must be given before phase transfer kinetics are neglected.

Cases where an equilibrium model does not apply have been reported for aqueous systems. Adsorption equilibrium for some VOC on aqueous sediments can take from days to months (Wu and Gschwend,1986; Karickhoff, 1984). Wu and Gschwend (1986) reported cases where physical mixing processes exposed sediments to contaminants at rates exceeding mass-transfer rates. Under such conditions the equilibrium assumption will not apply.

However, in soil systems, the use of an equilibrium model is probably justified since there is evidence that equilibrium proceeds rapidly. In experiments by Chiou and Shoup (1985) on

the gas-phase adsorption of five VOC onto soil, sorption equilibrium was generally achieved within four hours. Soil gas motion due to observed basement underpressures occurring during normal house use is very slow. For example, around houses which are well coupled with the soil a pressure differential of a few Pascal might develop over several meters of soil. In highly permeable soil (10^{-9} m^2), the soil gas velocity would be only on the order of one cm-hr^{-1}. Under such conditions the equilibrium assumption would be expected to apply. In the case of the migration of landfill gas equilibrium might not apply within the fill, however off site where the pressure gradient is equilibrium transport would be established.

Soil gas motion due to the basement underpressures For VOC in soil gas near houses Therefore, under the low flow regimes an equilibrium model is probably justified.

The one-dimensional model derived here is applicable to the soil column experiments discussed in Chapter 3. The model's three-dimensional equivalent would apply to the gas-phase migration of VOC from a landfill under the influence of a pressure gradient due to the buildup of methane gas, or to the migration of VOC from a leaky underground storage tank under the influence of the pressure field around the basement of a house.

Darcy's Law

Pressure-driven flow of fluid through a porous medium, such as soil, is governed by Darcy's Law. For a gas, the one-dimensional equation has the form:

$$v_d = \frac{-k}{\mu}\frac{dP}{dx}, \qquad (2.1)$$

where v_d, referred to as the Darcy velocity, is the volumetric gas flux resulting from the pressure differential dP/dx, k is the intrinsic permeability of the soil, and μ is the absolute viscosity of the gas. It should be noted that v_d is the approach velocity of the gas to the porous medium. The average flow velocity in the medium, v_x, is faster, such that $v_x = v_d/a$, where a is the air-filled fraction of the soil.

Darcy's Law applies under conditions of laminar flow. This criteria is satisfied if the Reynold's number, Re, does not exceed some number between 1 and 10. Bear (1972) reports that, for porous media, Re takes the form:

$$Re = \frac{v\,d}{\nu}\ , \qquad (2.2)$$

where v is the fluid velocity and ν is the kinematic viscosity (absolute viscosity/fluid density). The parameter d, characteristic of the grain dimension, has different accepted forms. Sometimes d_{10} (or d_{50}) is used, defining the size, d, such that 10 (or 50) percent of the mass of the soil has grain size less than d. For soil air ν is 0.2 cm^2s^{-1} under ambient conditions.

Fick's Law

Molecular diffusive in air is governed by Fick's Law:

$$F = -D_a\, dC_a/dx \qquad (2.3)$$

where F is the mass flux, D_a is the diffusion coefficient of the contaminant in air, and dC_a/dx is the contaminant concentration gradient in air. In order to account for the increased path length of a molecule diffusing in soil, D_a is divided by a tortuosity factor τ, to obtain an effective diffusion coefficient:

$$D_{eff} = D_a/\tau\ . \qquad (2.4)$$

τ is always greater than 1 and can be greater than 2 (Hillel, 1980, pg. 177). Typical values for tortuosity in soil are 1.5 or 1.6.

Equilibrium Partitioning of VOC

VOC of interest as environmental contaminants have low water solubilities, have high vapor pressures, are uncharged, and are relatively nonpolar. These properties govern their partitioning behavior among the three phases of the soil medium. Air-water partitioning in

soil is governed by Henry's Law. Air-solid and water-solid partitioning are more complex phenomena. Chiou *et al.* (1988) conducted experiments which indicate that the soil acts as a two phase medium, such that VOC sorption to the solid phase can occur via mineral surface adsorption or by absorption into soil organic matter.

Contaminant partitioning between the aqueous and vapor phases at low aqueous concentrations is described by Henry's Law:

$$C_a = H\, C_w, \tag{2.5}$$

where, C_a is the concentration of the contaminant in air, C_w is the concentration in water, and H is Henry's Law constant. Henry's Law constants are experimentally determined or can be estimated from vapor pressure and solubility data. For VOC which are low-solubility liquids at ambient temperatures, H is obtained by dividing the vapor pressure of the pure liquid by its solubility in water, where both quantities are taken at the system temperature. In practice, there has been considerable confusion over the calculation of Henry's Law constants for compounds which are gases under ambient conditions, in which case Henry's Law can be estimated by dividing ambient pressure (rather than the vapor pressure of the pure liquid) by the solubility of the gas at one atmosphere. Mackay and Shiu (1981) provide a detailed reference on the proper calculation of Henry's Law constants and compile Henry's Law constants for many VOC important as environmental contaminants.

Historically, partitioning between the solid and fluid phases has been explained as a surface-adsorption phenomenon. Chiou *et al.* (1979) first suggested that partitioning of aqueous-phase non-ionic organic compounds into soil organic matter was a dissolution (absorption) process rather than a surface adsorption phenomenon. Water-solid partitioning was found to be linear and correlated with the weight fraction of organic carbon in the soil, such that:

$$C_s = f_{oc}\, K_{oc}\, C_w, \tag{2.6}$$

where C_s is the concentration of VOC on the solid phase, f_{oc} is the weight fraction of organic carbon in the soil, and K_{oc} is the temperature-dependent, contaminant-specific adsorption

coefficient.

Few direct measurements have been made of sorption coefficients for the myriad VOC found as environmental contaminants. Correlations have, however, been found between the sorption coefficient and compound solubility in water, S. Lyman *et al.* (1982, Chapter 4) provide an excellent summary of these studies all, of which report a relationship of the form:

$$\log K_{oc} = a + b \log S. \qquad (2.7)$$

Most of the reported regressions are, however, based on pesticide data. Because pesticides are expected to be more persistent on soils, these data regressions are probably not be a good model for the behavior of VOC.

Chiou *et al.* (1979) measured K_{oc} for 15 chlorinated hydrocarbons (two of which were low mass VOC) and obtained the following relationship:

$$\log K_{oc} = 4.277 - 0.557 \log S , \qquad (2.8)$$

with a coefficient of determination (r^2) of 0.99, where S has units of micromole L^{-1}, and K_{oc} is unitless. (The original form of Chiou's equation was rewritten as a function of K_{oc} in the manner suggested by Lyman *et al.* (1982, pp. 4-9).)

Chiou and Shoup (1985) demonstrated the importance of mineral surface adsorption in dry soils in a series of experiments in which the vapor-phase uptake of VOC onto soil was determined as a function of relative humidity (RH) of the soil gas. Their work indicates that the soil acts as a dual sorbent from the gas phase. The intrinsically charged mineral surface and the soil organic matter provide two types of sorption sites with distinctly different properties. The mineral surface acts as a conventional surface phenomenon adsorber, while the the organic fraction absorbs organic contaminants (Chiou *et al.*, 1988). The authors found that at low RH VOC sorbed to both the mineral surface and the organic fraction. Sorption isotherms measured at low test-gas RH were found to be distinctly nonlinear. At higher RH water vapor began to displace VOC on the mineral surface sites. At RH greater than 90 percent, VOC sorption was essentially confined to the organic fraction, with total sorption

significantly lower than at low RH. The normalized vapor-phase isotherms (C_s vs. P/P_{sat}) had fallen into the range of aqueous isotherms (C_s vs. $C_w/C_{w,sat}$), where P_{sat} and $C_{w,sat}$ represent the saturation vapor pressure and the saturation water solubility, respectively.

RH in natural soils are normally 98 - 100 percent, with air-dry soils at approximately 50 percent due to the retention of capillary water (H. Donner, UCB, personal communication). Therefore, the soil characteristic dominating sorption of VOC in the natural environment should be the organic carbon content. This considerably simplifies the transport analysis in that: 1) the analytically simpler, linear-sorption isotherm may be used; and 2) vapor-solid sorption need not be considered separately from water-solid sorption. Accordingly, substitution of Equation 2.5 into Equation 2.6 gives the solid-vapor partitioning equation:

$$C_s = (f_{oc} K_{oc}/H)C_a. \qquad (2.9)$$

For completeness one further point should be discussed about VOC sorption by organic matter. Research by Karickhoff *et al.* (1979) indicates that not all organic carbon behaves in the same manner. The authors investigated sorption of hydrophobic compounds onto different particle size fractions of pond and river sediments. They found the organic fraction on sands to be 50-90 percent less effective a sorbent than the organic carbon on the silt and clay fractions. This effect will be neglected in this paper because the uncertainty in the predicted adsorption coefficients and due to soil inhomogeneity are expected to be at least as large as those resulting from the difference in organic carbon behaviour of the various particle size fractions.

The Time Dependent Advection-Diffusion Equation

Using the equilibrium partitioning relationships, the time dependent advection-diffusion equation can be derived for the motion of a gas-phase contaminant through soil. The soil is treated as a three-phase medium with n as the porosity (volume of non-solid/volume of soil) and s the water filled fraction of n (volume of water/pore volume). Typical soil porosity is

usually in the range of 0.3 to 0.6 (Hillel, 1980, pg. 11). The water filled fraction is more variable and is time dependent.

The one-dimensional partial differential equation is derived through mass balance. For a given volume element the mass entering by advection, at velocity v_x, plus by diffusion, with flux F_{eff} (where $F_{eff} = D_{eff} dC_a/dx$), is set equal to the mass leaving by advection and diffusion plus the change in concentration in each of the three phases.

$$C_a(x)v_x An(1-s)\Delta t + F_{eff}(x)n(1-s)A\Delta t =$$
$$C_a(x+\Delta x)v_x(x+\Delta x)An(1-s)\Delta t + F_{eff}(x+\Delta x)n(1-s)A\Delta t +$$
$$\Delta C_a(x)n(1-s)A\Delta x + \Delta C_w(x)nsA\Delta x + \Delta C_s(x)\rho_b A\Delta x ,$$

Where A is the area of the volume element, Δx is the element width, Δt is the time increment, and ρ_b is the bulk density of the soil. $F_{eff}(x)$ and $F_{eff}(x+\Delta x)$ represent the diffusive fluxes entering and leaving the element, respectively. The same convention is followed for the concentrations. The last three terms on the right hand side are the changes in concentration in each of the phases, air, water, and solid, of the volume element. Substituting in Equations 2.3, 2.5, and 2.9, rearranging terms, and taking the limit in which Δx and Δt go to zero, gives the advection-diffusion equation:

$$\frac{\partial C_a}{\partial t} = \frac{-1}{R}\frac{\partial (C_a v_x)}{\partial x} + \frac{D_{eff}}{R}\frac{\partial^2 C_a}{\partial x^2} , \qquad (2.10)$$

where,

$$R = 1 + \frac{s}{H(1-s)} + \frac{\rho_b f_{oc} K_{oc}}{Hn(1-s)} . \qquad (2.11)$$

Assuming a constant advective velocity,

$$\frac{\partial C_a}{\partial t} = \frac{-v_x}{R}\frac{\partial C_a}{\partial x} + \frac{D_{eff}}{R}\frac{\partial^2 C_a}{\partial x^2} . \qquad (2.12)$$

The first term on the right-hand-side is the advective contribution to transport, while the second term is the contribution by molecular diffusion. the form of Equation 2.12 suggests the function of R, the retardation factor. It is the factor by which contaminant velocity is slowed with respect to the bulk soil-gas velocity. The coefficient of the diffusion term shows that R also serves to increase the diffusion time. As can be seen from Equation 2.11, a large adsorption coefficient combined with a small Henry's Law constant can result in a large contaminant retardation. Notice that since both H and K_{oc} are temperature dependent, and since s is subject to temporal variation, R will not remain constant throughout time.

Using the Peclet number, Pe, from fluid mechanics one can simplify Equation 2.8 for problems in which either diffusion or advection can be neglected.

$$Pe = \frac{v\,L}{D} \quad , \tag{2.13}$$

where, in porous media, v is the velocity of the bulk fluid, D is the effective diffusion coefficient of the compound of interest, and L is the scale of interest in the problem. For example, in the soil column experiments of Chapter 3, L is the length of the column. For Pe much greater than one, diffusion can be neglected. If diffusion can be neglected, and advection is governed by Darcy's Law, then, from Equation 2.12, the equation for pressure-driven flow of VOC in soil becomes:

$$\frac{\partial C_a}{\partial t} = \frac{-v_d}{R} \frac{\partial C_a}{\partial x} \quad . \tag{2.14}$$

In summary the theory of fluid mechanics and the equilibrium partitioning behavior of VOC have been used to derive the equation of the gas-phase, pressure-driven transport of VOC through soil. The derivation of the equation results in a retardation factor which tells how fast the contaminant front moves with respect to the bulk soil-gas velocity. Since the equilibrium partitioning equations are temperature dependent, and the soil parameters can be

time dependent, the retardation factor is subject to temporal and meteorological variations. In the case of soil-gas contamination in the vicinity of a house, meteorologically induced repartitioning could result in temporal variation in the soil-gas source of VOC.

CHAPTER 3

SOIL COLUMN EXPERIMENTS

INTRODUCTION

In this phase of the study an experimental apparatus and a method were designed for the direct observation of pressure-driven flow of VOC under controlled laboratory conditions. The goal was to develop aprocedure simple enough to be used for rapid screening of the mobility of important landfill gas contaminants under advective flow conditions. The apparatus and method were used to compare the mobility of two tracer-gases (sulfur hexafluoride and hexafluorobenzene) proposed for use in field investigations of the advective flow of soil gas. The retardation factors of the two compounds were measured and compared with the theoretical retardation factor derived in Chapter 2. A comparison of tracer-gas transport in wetted and air-dry soil enabled a qualitative comparison between mineral surface adsorption and organic carbon sorption.

The apparatus and method developed for these experiments can be applied to the study of long-distance transport of VOC through soil. The retardation factors which are measured are applicable to a situation in which contaminated soil gas moves into a region of soil not already in equilibrium with the inflowing gas. For example, in the case of gas-phase VOC migrating away from a landfill on a methane gas plume, the relative retardations of various VOC, give an estimate of which VOC will move the farthest and fastest through the soil.

The procedure described in this chapter can also be useful for estimating temporal variations in the concentration of VOC in soil gas. For rapidly equilibrating VOC, the measured retardation factors can be used to determine the soil sorption coefficient (Equation 2.11). This information in conjunction with knowledge of temporal variations in soil conditions (temperature and water content) can be used to estimate changes in the concentration of VOC in soil air. The soil column experiments are not directly applicable to the field

experiments on VOC inflow into a basement because of the short time scale of the experiment and the short distances through soil over which soil gas is induced to flow.

METHODS

Soil Column Apparatus

A soil-column apparatus was designed to achieve the goals outlined above. The particular design objectives were as follows. The apparatus was designed to have low reactivity, to be noncontaminating, and to allow the interchange of columns of soil of various lengths. A regulated flow of test gas was to be passed through the column while measuring the flow-rate and pressure difference across the soil. The test gas would be controlled and monitored for relative humidity, and concentration of VOC in the outlet gas would be monitored at near real-time. The soil column was to be packed homogeneously and in a reproducible manner and soil characteristics were to be varied by the use of different soils.

Figure 3.1 is a schematic diagram of the soil-column apparatus. The apparatus consists of three nickel-plated brass sections. The central section is the soil column itself. Constructed of 9.4-cm id pipe, it is screened on the bottom with 50 micron stainless steel mesh. Columns of various lengths were built to facilitate observation of compounds with different retention times. The mesh, which supports the soil, is fine enough to contain the clays in a static environment after soil packing, but offers no significant resistance to test-gas flow. The top and bottom extensions, sealed to the central column via Viton O-rings set into bolted flanges, provide ports for test gas entry and exit and pressure probes. The importance of careful temperature control was not realized until near the end of the tracer-gas experiments. At that time temperature probes were added to the extensions above and below the soil column in order to correlate observed effects with temperature.

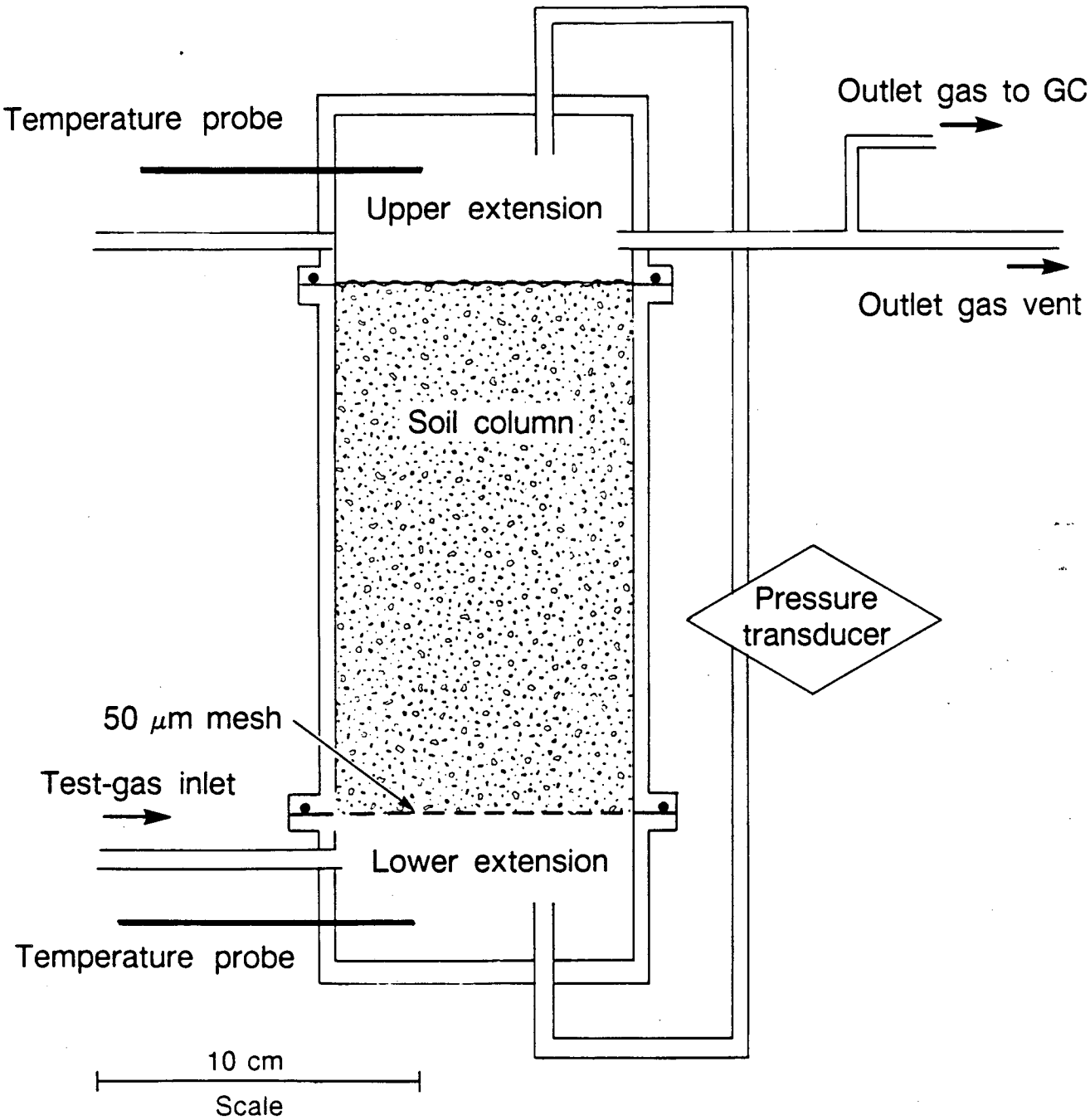

Figure 3.1. Diagram of soil-column apparatus.

Soil Characterization

Three Northern California soils were collected to represent a range of particle-size distributions and organic carbon contents. They were Panoche Soil, Yolo Loam, and Delhi Sand. Soils were thinly spread and air dried for several days and then passed through a 2-mm sieve. Each soil was analyzed for particle-size distribution and organic carbon content. Particle-size distribution was determined by the standard hydrometer-method sedimentation analysis for clay and silt, and by sieving for sand (Day, 1965). Soil organic carbon content was measured using the Walkley-Black procedure (Nelson and Sommers *et. al*, 1982). The method uses dichromate ion from $K_2Cr_2O_7$ to oxidize soil organic carbon. The dichromate remaining unoxidized is determined by titration with Fe(II). The organic carbon fraction is then determined from the difference between total and unoxidized dichromate.

Soil Packing

Soil columns were packed using a mechanical device based on the design of Reeve and Brooks (1953), illustrated in Figure 3.2. An extension is bolted onto the top of the soil column. Soil is dropped into the extension-column assembly from a reservoir with a perforated bottom. While the soil is falling, the perforated bottom is rotated, resulting in an evenly distributed, lightly packed soil. The column and extension are then fastened onto a platform and light pressure is applied to the top of the soil with a spring. The entire assembly is then repeatedly dropped 2.5 cm onto a rubber covered platform, driven by the spiral cam. The extension is then rotated off of the column leaving a smooth soil surface, and a homogeneously packed sample.

Soil Wetting

In order to vary the water content of the soil while leaving all other soil variables unchanged, several methods of wetting pre-packed soils were attempted. Passing air saturated

with water vapor through the soil column was unsatisfactory because of the excessive length of time required to wet the soil. Methods in which water was added directly to the column also proved to be unsatisfactory because soils treated in this manner contracted from the walls of the column leaving a short circuit for the test gas to flow around the soil.

The following procedure was, therefore, adopted of wetting the soil before packing. Several kilograms of air dry soil were divided into four parts and spread thinly on a heavy plastic sheet. The soil in each of the four parts were then sprayed with a fine mist of water and stirred. This process was repeated just to the point were visible clumping began. The four parts were then mixed and placed in a vapor-proof container and tumbled on a roller over night to condition the soil. In the morning the soil was removed from the container and passed though a 2-mm sieve. Packing of the column proceeded as described above, resulting in a uniformly packed, low-density, highly permeable soil. The moisture content of the soil was determined by weighing a sample of the wetted soil before and oven-drying at 110 °C to constant weight.

Measurement of Soil Permeability

After assembling the packed soil columns (as in Figure 3.1), soil permeabilities were measured by passing a regulated flow of pure air through the column while monitoring the pressure drop across the soil. The pressure was measured with a variable reluctance pressure transducer (Model DP103, Validyne Instr., Inc.) and gas flow rates were regulated and monitored by mass flow controller. For one dimensional flow the expression for permeability may be obtained directly from the one-dimensional form of Darcy's Law (Equation 2.1). Here the flux was rewritten in terms of the volumetric flow rate (Q) per soil column area (A) resulting in:

$$k = \frac{-\mu Q}{A} \frac{\Delta L}{\Delta P}, \qquad (3.1)$$

where k (cm^2) is the intrinsic permeability, μ (1.84×10^{-4} g cm^{-1} s^{-1}) is the viscosity of air,

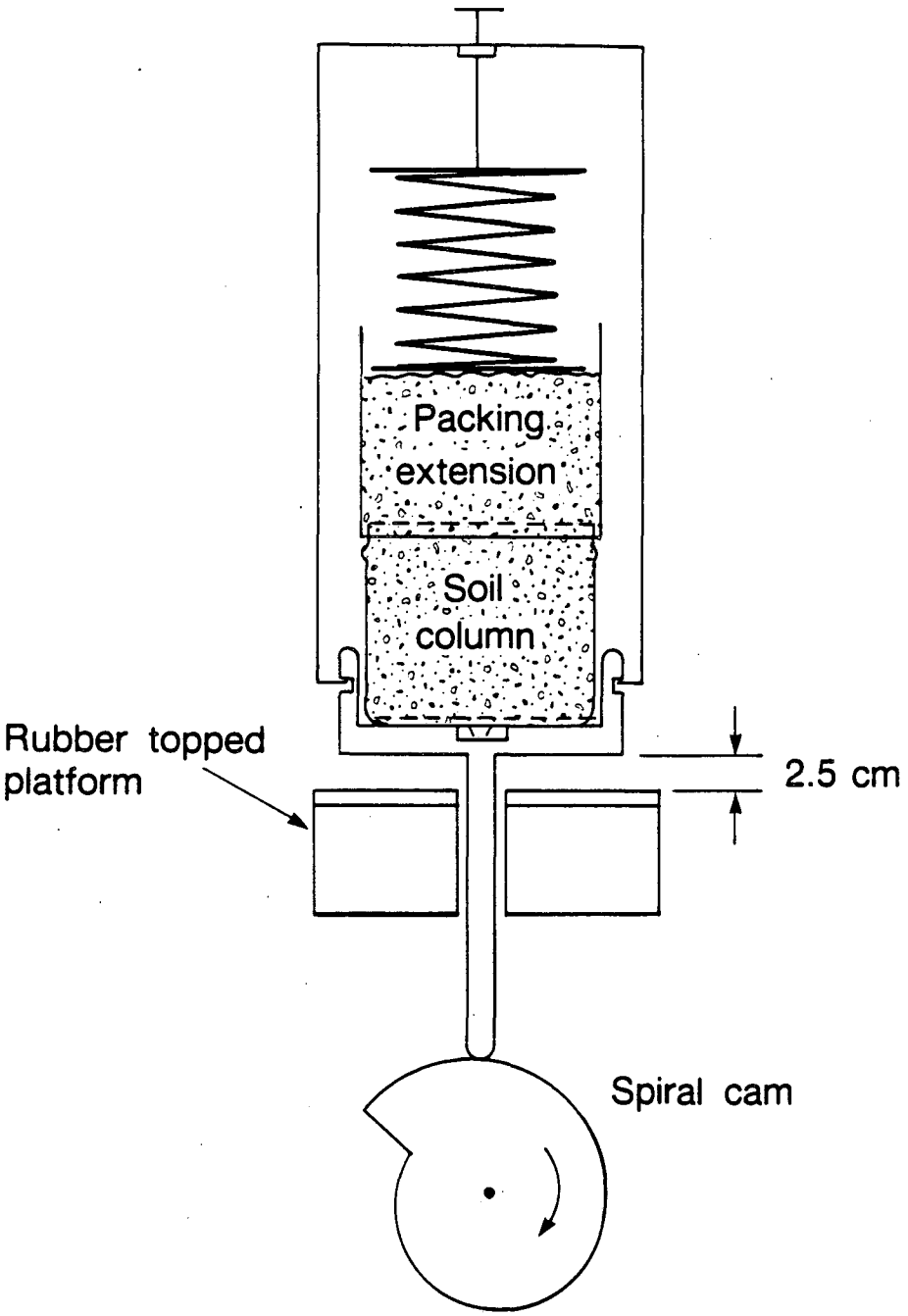

Figure 3.2. Diagram of soil-packing device. From Reeve and Brooks (1953).

Q ($cm^3\ s^{-1}$) is the test-gas flow rate, A (cm^2) is the area of the soil column, ΔP (dyne cm^{-2}) is the pressure drop across the column, and ΔL (cm) is the height of soil equal to the column length.

Preparation of Test Gases

The test gases were prepared for the transport experiments in the following manner. HFB gas was prepared by diluting a small injection of pure HFB liquid with pure air to 100 ppm in a Tedlar gas-sample bag. The SF_6 tracer was a commercially prepared, pressurized mixture of 190 ppb SF_6 in pure air. Test-gases to be passed through wetted soils were humidified before entry into the soil column by passing the gas stream over boiling water, and then through a condenser and glass wool to filter out liquid-phase water. The outflow from the condenser was then passed through a coil of Teflon tubing to equilibrate the test gas to ambient temperature before inletting to the soil column. The relative humidity of the gas stream, was measured periodically during the transport experiments both upstream and downstream of the soil column by dewpoint hygrometer (Model 911, EG&G, Inc.).

Analysis of Test-Gas Concentrations

Tracer gas concentrations were measured with a gas chromatograph (GC) (Model 1030A, Baseline Industries, Inc.) equipped with an electron capture detector (ECD). The GC was set to sample automatically at one minute intervals. The GC was configured with two ten-port valves to accommodate simultaneous operation of two columns, one for SF_6 and the other for HFB. A molecular sieve (5A) column (0.32 cm OD, 0.22 cm ID x 2.4 m) was used for SF_6. The HFB column was 100/120 mesh Chromosorb G with OV 101 silicone coating (0.32 cm OD, 0.22 cm ID x 0.41 m). The GC was operated isothermally at 150 °C with the detector at 240 °C. The carrier gas was Argon with 7 percent methane, and was run at a flow rate of 50 $cm^3 min^{-1}$. Under these conditions, the retention times were 5 seconds for HFB and 28 seconds

for SF_6.

Peak height rather than peak area was used for the calibration of the two test-gases. The concentration of SF_6 was linear with peak height up to 200 ppb, with a resolution of 0.5 ppb. The concentration of HFB was was nonlinear with peak height up to 8 ppm, and linear between 8 and 100 ppm. At low concentrations (below 8 ppm) peaks broadened before increasing in height. For the purposes of the soil-column experiments, the nonlinearity at low concentrations did not interfere with the analysis, and was therefore ignored.

Experimental Setup and Procedure for Transport Experiments

Figure 3.3 is a schematic of the setup for the transport experiments. The flow rate of the test gas entering the soil column was maintained at 100 cm^3 min^{-1} using an electronic mass flow controller (0 - 100 cm^3 min^{-1}). This flow rate resulted in stable pressure differentials across the soil various soil of between two and 24 Pascal, as determined by a variable reluctance pressure transducer (Model DP103, Validyne Instr., Inc.). One test gas at a time was introduced to the soil column. Either SF_6 was delivered under pressure to the mass flow controller from a gas cylinder, or HFB, contained in a gas-sampling bag, was delivered to the mass flow controller with a peristaltic pump and an in-line 5-L pressure capacitor to dampen pressure fluctuations due to the pump. The gas-stream then either passed through the humidifier (for experiments in wet soils) or by passed it (for experiments in dry soils) before entering the soil column. Test-gas exiting the soil was sampled by GC with the excess vented to the laboratory hood.

The transport experiment was initiated by introducing the test gas through a port in the base of the soil-column apparatus at time zero. While test gas exiting the column was monitored by GC-ECD, the flow rate of the test gas and the pressure across the soil were monitored as in the soil permeability measurements. During long experiments (those lasting many hours) inflow concentrations were periodically checked. When outflow concentrations

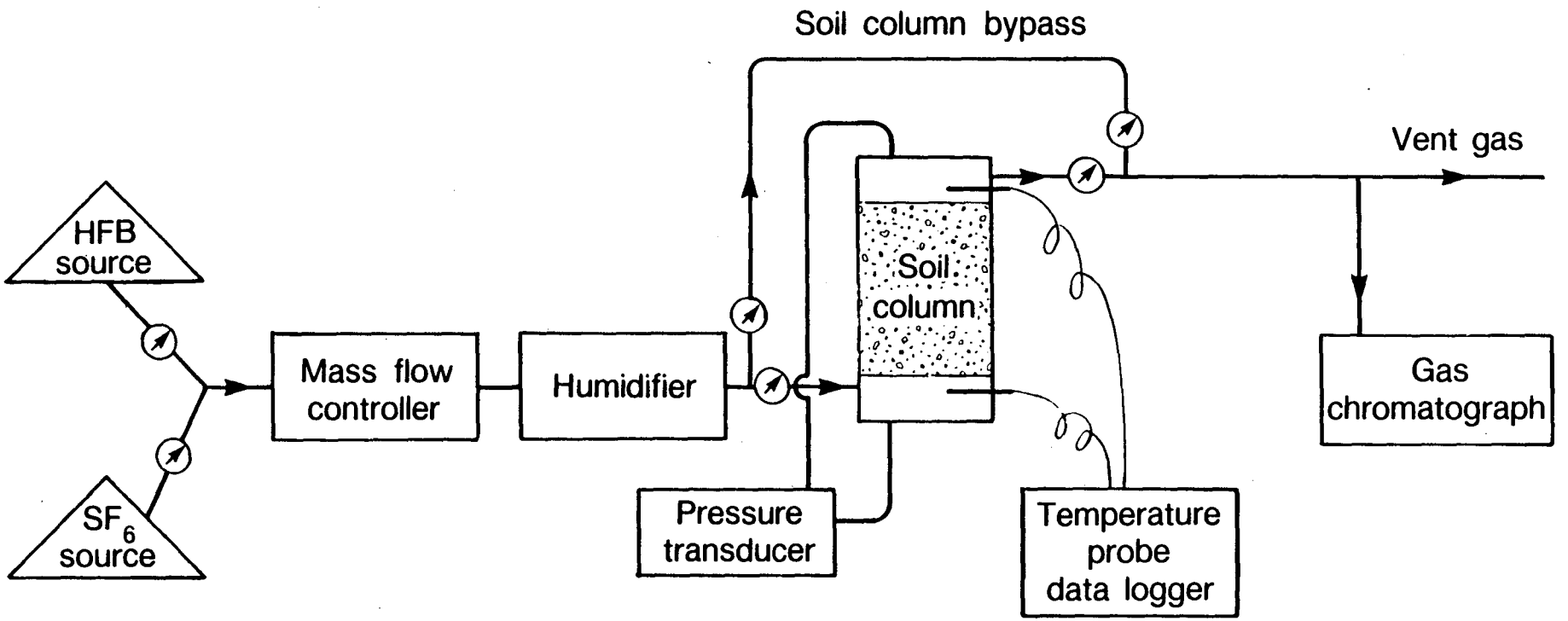

Figure 3.3. **Schematic diagram of experimental setup.**

were equal to inflow concentrations pure air was substituted for the test gas and the decay in concentration at the soil-column outlet was monitored over time.

Experiments were performed during which first SF_6 and then HFB were passed through the soil column packed with air-dry Delhi Sand, air-dry Yolo Loam, and air-dry Panoche Soil, and Panoche Soil with 8.6 percent water by weight. A 5-cm long soil column was used in each case to minimize the time required for the concentration of the outlet gas to equal the concentration at the inlet. In these experiments a common test-gas flow rate (100 cm^3min^{-1}) was used in order that tracer retardation factors might be compared directly.

RESULTS AND DISCUSSION

Soil Characterization

Table 3.1 summarizes the results of the soil particle-size distribution and organic carbon analysis. Unfortunately, all soils were found to be quite low in organic carbon. There was, however, a considerable spread in organic carbon content, with Panoche Soil and Yolo Loam having about 0.2 percent by weight, and Delhi Sand having 0.03 percent. All of the soils had sand contents of 69 percent or more. There was a reasonable spread in clay content from Panoche Soil at 17 percent, to Delhi Sand at 3 percent. The cumulative grain size distributions of each of the soils is presented in Figure 3.4.

Soil Packing

The standardized soil-packing procedure (using the spiral cam soil packing device) produced satisfactorily reproducible soil packing. The reproducibility of packing was assessed by making permeability measurements of the packed columns. Figure 3.5 shows soil permeability versus number of impacts used to pack Yolo Loam in a 16-cm soil column. By

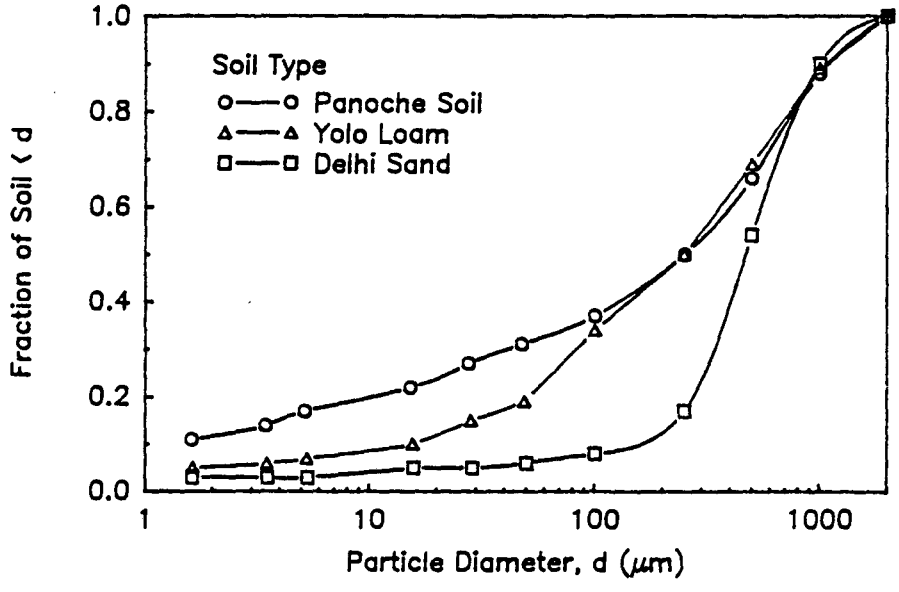

Figure 3.4. Cumulative particle-size distributions of soils.

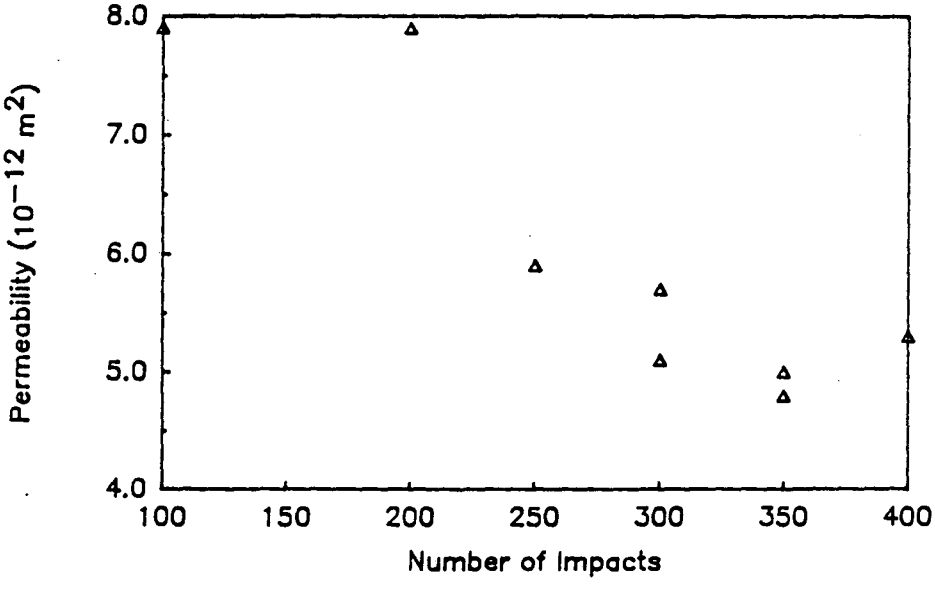

Figure 3.5. Permeability of Yolo Loam in 16-cm column versus number of impacts.

Table 3.1. Particle-size fractions and organic carbon content of soils by weight.

Soil	Clay (%)	Silt (%)	Sand (%)	OC[a] (%)
Panoche Soil	17	14	69	0.24
Yolo Loam	7	15	78	0.23
Delhi Sand	3	3	94	0.03

a. organic carbon

Table 3.2. Measured breakthrough times of SF_6 and HFB for pressure-driven flow across a 5-cm soil column.

Soil	Soil Water (%)	k[a] (m^2)	τSF_6[b] (min)	τHFB[b] (min)
Panoche Soil	AD[c]	2×10^{-11}	11	340
Panoche Soil	8.6	1×10^{-11}	10	15
Yolo Loam	AD	1×10^{-11}	10	720
Delhi Sand	AD	2×10^{-11}	11	60

a. Permeability

b. Time for outlet concentration to reach $1 - e^{-1}$ of inlet concentration

c. Air dry

this criterion packing was found to be reproducible to approximately 10 percent when 350 or more impacts were used. Consequently, 400 impacts was used to pack the soil for the transport experiments.

Soil Permeability

The permeability of air-dry Yolo Loam in a 16-cm column was measured at various applied pressures. As shown in Figure 3.6, the apparent Darcy permeability calculated using Equation 3.1, decreased with increasing applied pressure. In another experiment using Yolo Loam with 1.9 percent water in a 16-cm column, permeability was found to increase with increasing applied pressure (Figure 3.7), however, the magnitude of the effect was smaller than for experiments on air-dry soils. Additional experiments using soils with higher water contents, Panoche Soil with 8.6 percent water and Yolo Loam with 8.8 percent water, both in a 5-cm column, showed no systematic trend of permeability with applied pressure.

According to the original form of Darcy's Law, soil permeability should be constant with applied pressure. Seeking an explanation for the deviations of the observed permeabilities, three calculations were made to ensure that Darcy's Law applied to the experimental system. First, the Reynold Number was calculated using Equation 2.2. With d = 100 μm, ν = 0.144 $cm^2\ s^{-1}$, and v_x = 0.06 cm s^{-1}, corresponding to the highest flow rates used in the experiments, Re is 4 x 10^{-3}, well within the laminar flow regime. Second, the permeability data were entered into the Equation of Darcy's Law for a compressible gas to determine if compressibility of the test gas could account for the observed deviation. From Scheidegger (1974):

$$v = \frac{-k}{\mu} \frac{(P_t^2 - P_b^2)}{2 P_b L}, \qquad (3.2)$$

where P_b and P_t are the pressures at the bottom and top of the column, respectively. Even at a pressure of 400 Pa, well above that applied in the experiments, the correction for

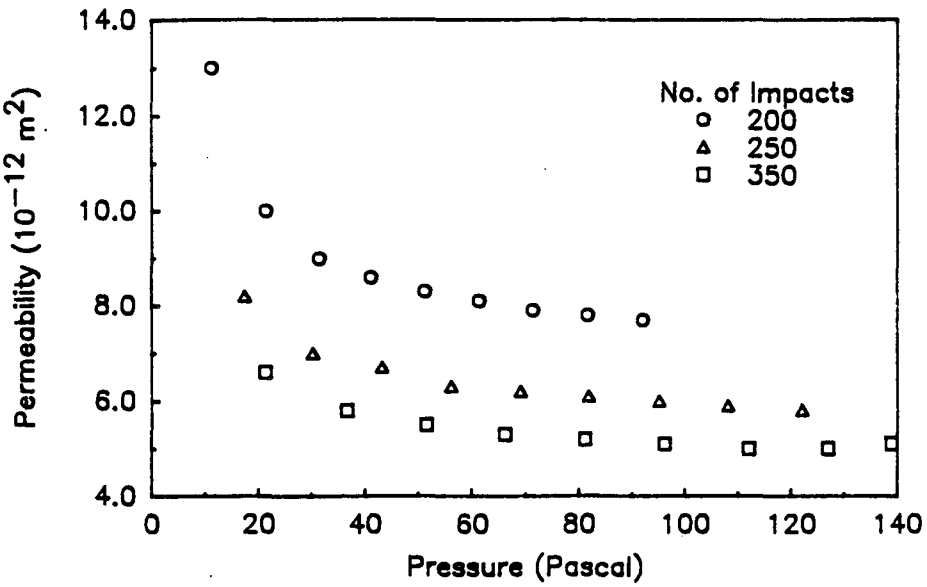

Figure 3.6. Permeability of air-dry Yolo Loam in 16-cm column versus pressure differential across column.

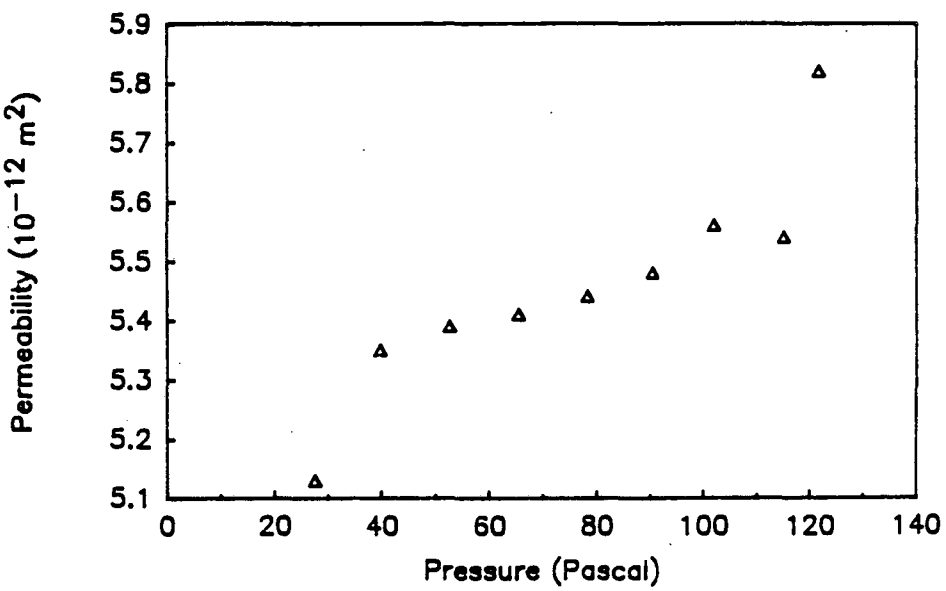

Figure 3.7. Permeability of moist Yolo Loam (1.9 percent water) in 16-cm column versus pressure differential across column.

compressibility is only 0.2 percent, which does not explain the observed deviation. Third, the hypothesis of imperfect fluid viscosity at the soil surface was tested. Klinkenberg (1941), assuming the fluid to have small, but finite velocity at the media surface, calculated the relationship between the apparent and true permeabilities:

$$K_a = K (1 + b/P) \qquad (3.3)$$

where K is the true, constant permeability, K_a is the measured permeability, and P is the mean pressure of the gas in the column. A plot of experimental values of K_a versus 1/P does not linearize the data and, therefore, the Klinkenberg effect does not account for the observed deviations.

Data similar to those in Figure 3.6 have also resulted from in-situ permeability measurements (Turk, et al., 1987; R. Sextro, unpublished data). Our conclusion is that the effect is due to a change in the porous medium itself. We hypothesize that as applied pressures are increased in dry soil, the fine particles are forced into the interstices of the medium resulting in a systematic increase in resistance to flow. Resistance will become asymptotic at high pressures when no more rearrangement can occur. This effect is reduced in wetter soils as the fine particles become aggregated in the presence of water. The increase in permeability with pressure, shown in Figure 3.7, might result when water contained in the pore spaces is redistributed at elevated pressures.

For environmental applications, however, the uncertainty in the measured permeability resulting from the effect described above will, in general, be insignificant. A two- or three-fold uncertainty due to variation in measurement technique can be tolerated in a parameter which ranges over seven orders of magnitude. In addition, the variation in permeability due to small scale heterogeneity in natural soils is undoubtedly larger than the measurement uncertainty.

Comparison of SF_6 and HFB

Table 3.2 compares the measured breakthrough times of SF_6 and HFB for pressure-driven transport through the various soils. The breakthrough time is defined as the elapsed time from the onset of the experiment for the concentration of the compound at the outlet of the column to reach $1-e^{-1}$ of the concentration at the inlet. Figures 3.8 through 3.13 show the concentrations of SF_6 and HFB at the outlet of the column for these experiments, where outlet concentrations have been normalized with respect to inlet concentrations. As discussed above, the anomalous signal of HFB at low concentrations are due to the nonlinearity of the calibration in that region.

In all of the experiments the transport of HFB was found to be retarded with respect to SF_6 (Table 3.2, Figures 3.8 - 3.13). This was most notable with the air-dry soils. For example, in air-dry Panoche Soil, the breakthrough time of HFB was a factor of 30 larger than that of SF_6 (Table 3.2), while in wetted Panoche Soil, there was less than a two-fold difference (Figure 3.13). This result is in agreement with Chiou and Shoup (1985) who found that, at the high soil-gas relative humidity expected in wet soils, water displaces hydrophobic organic compounds on mineral surface sites resulting in significantly decreased total sorption. Therefore, the large retardation of HFB in air-dry soil was probably due to mineral surface adsorption. Whereas the greatly reduced sorption in wetted soil is explained by uptake by the organic carbon fraction alone.

Assuming that the retardation of HFB in air-dry soil was due primarily to mineral surface adsorption, the greatest retardation would be expected in the soil with the highest clay content. Delhi Sand, with the lowest clay content of three percent, did produce the lowest retardation, but Yolo Loam, with 7 percent clay, produced higher retardation than Panoche Soil, with 17 percent clay (Table 3.2, Figures 3.8 - 3.12). The lack of temperature control during these experiments (discussed in more detail below) may account for this result.

A retardation factor was calculated for HFB using Equation 2.11 and the conditions of the

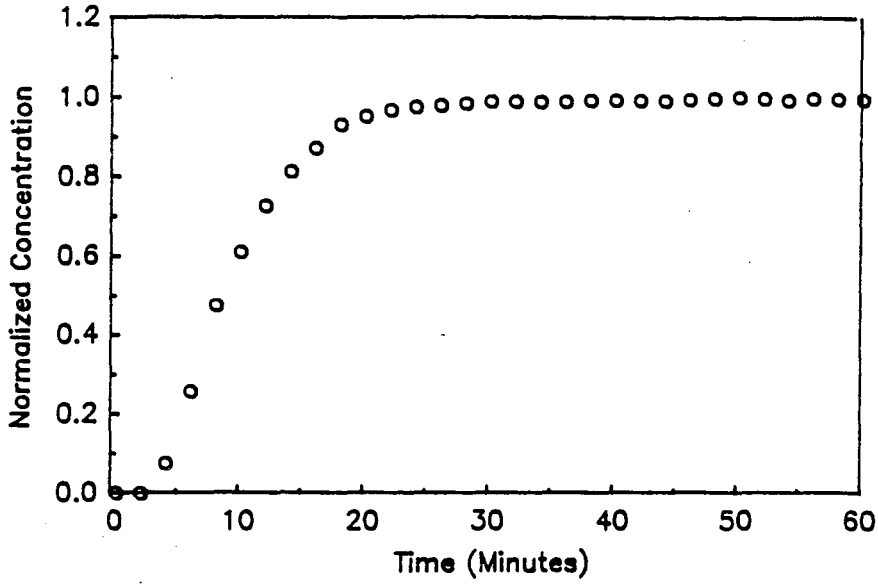

Figure 3.8. Breakthrough of SF_6 on air-dry Panoche Soil. The plot shows outlet concentration normalized to inlet concentration.

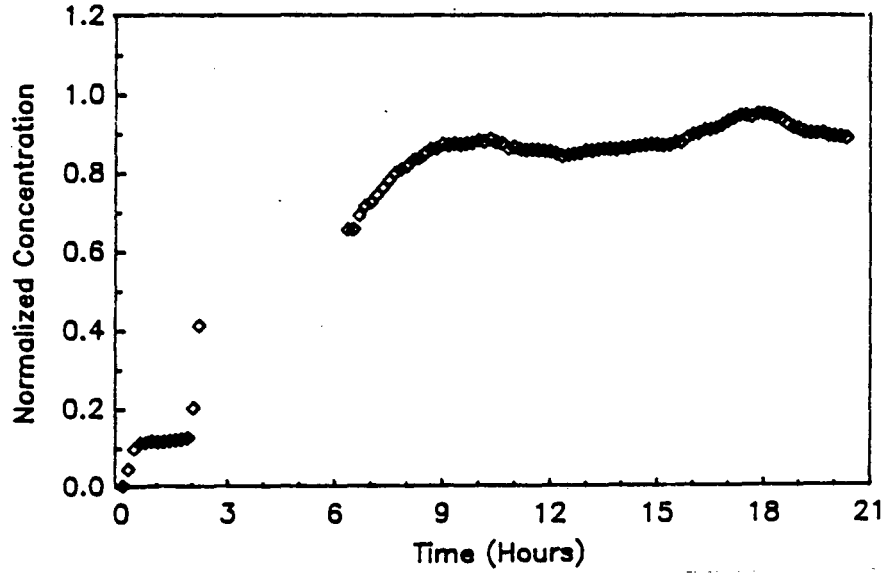

Figure 3.9. Breakthrough of HFB on air-dry Panoche Soil. The plot shows outlet concentration normalized to inlet concentration. Missing data points resulted from failure of GC automatic sampling valve.

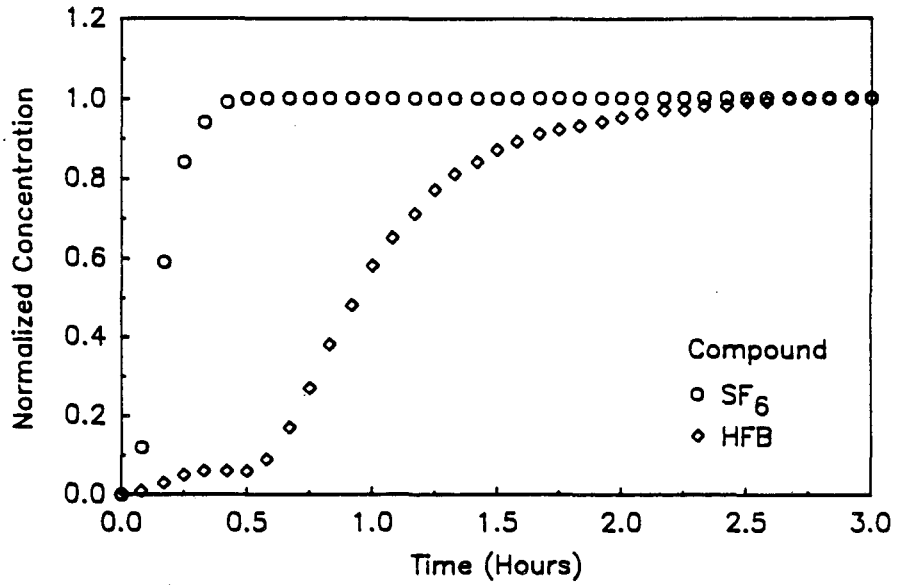

Figure 3.10. **Breakthrough of SF_6 and HFB on Dehli Sand. The plots show outlet concentrations normalized to inlet concentrations.**

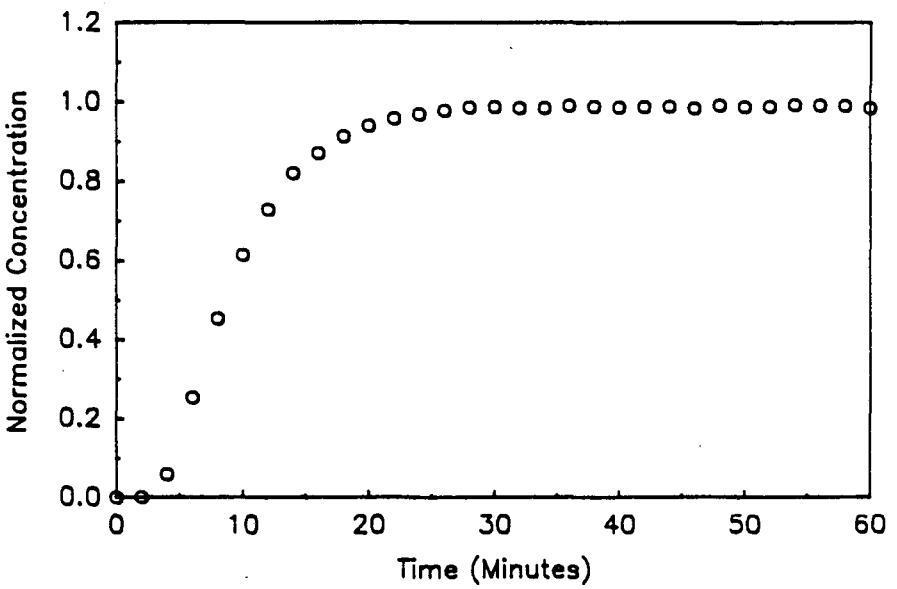

Figure 3.11. **Breakthrough of SF_6 on air-dry Yolo Loam. The plot shows outlet concentration normalized to inlet concentration.**

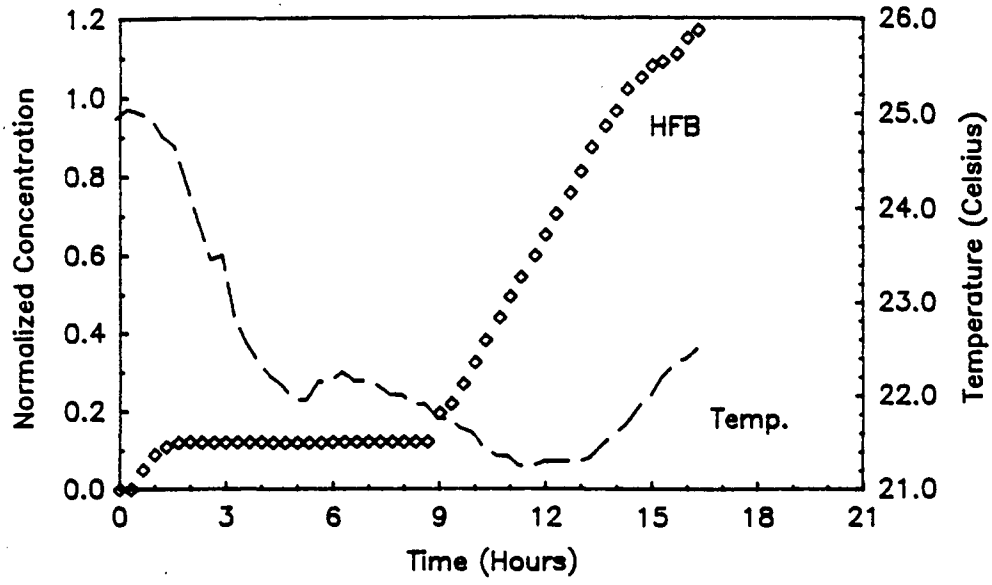

Figure 3.12. **Breakthrough of HFB on air-dry Yolo Loam. Outlet concentration normalized to inlet concentration is plotted along with average temperature of the soil column.**

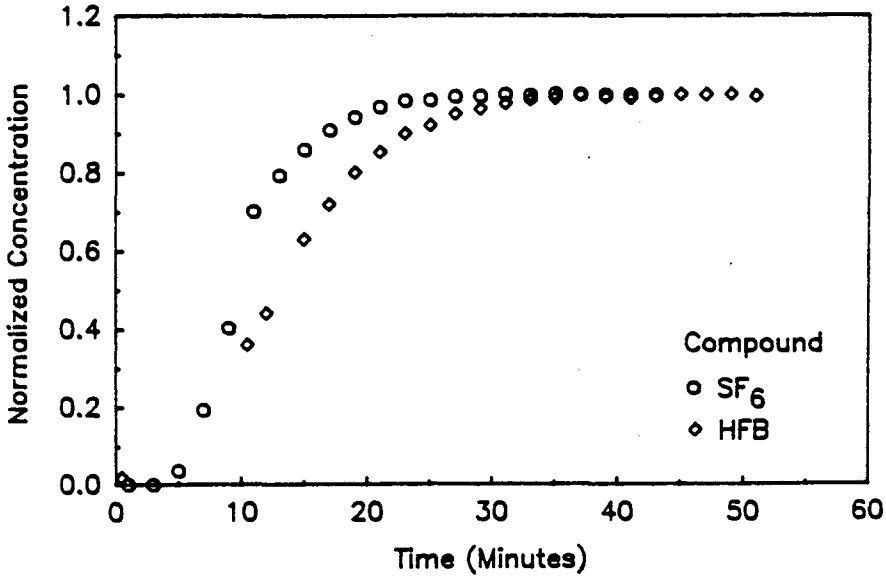

Figure 3.13. **Breakthrough of SF_6 and HFB on wetted Panoche Soil (8.6 percent water). The plots show outlet concentrations normalized to inlet concentrations.**

Table 3.3. Parameter values used to calculate theoretical retardation factor for HFB.

Parameter	Value	Source
n	0.4	estimated
s	0.25	estimated
ρ_b	1.12($g \cdot cm^{-3}$)	measured
f_{oc}	0.0024	measured
H	0.71[a]	*Eichler et al.*, 1986
K_{oc}	135[b]	calculated from Eq. 2.8 using data for S from *Eichler et al.*, 1986

a. The effective units of H are $cm^3 (H_2O)$-cm^{-1} (air).

b. The effective units of K_{oc} are $cm^3 (H_2O)$-g^{-1} (organic carbon), or equivalently, in unitless form, $g^3 (H_2O)$-g^{-1} (organic carbon).

experiment with wetted Panoche Soil. The numerical values of the parameters used in this calculation are presented in Table 3.3. The predicted retardation factor is 3.2. A retardation factor was also calculated for SF_6. Assuming K_{oc} for SF_6 equals zero, Equation 2.11 becomes:

$$R = 1 + \frac{s}{H(1-s)}. \qquad (3.4)$$

For a low solubility gas at atmospheric pressure, H can be calculated by dividing atmospheric pressure by the water solubility of the gas at one atmosphere (Mackay and Shiu, 1981). Using a solubility of 4.1×10^{-5} g(SF_6)-cm^{-3}(H_2O) at 20°C (Horvath, 1975), H is 150 cm^3(H_2O)-cm^{-3}(air), which makes the second term in Equation 3.4 negligible. Therefore, R for SF_6 can be taken as one, and SF_6 can be used as a reference gas against which to measure the retardation of HFB.

In order to obtain the experimental retardation of HFB relative to SF_6 a correction must be applied to the breakthrough-time data in order to account for the mixing time of the compounds in the soil-column extensions (Figure 3.1). The mixing time associated with the volume of the extensions, as determined by a well-mixed-box model, is V/Q, where V is the total volume of the extensions and Q is the flow rate of the test gas. Using Q from the experiment with wetted Panoche Soil, the mixing time is 6.9 minutes. Subtracting this time from the measured breakthrough time for SF_6 of 10.3 minutes (Table 3.2) results in an effective breakthrough time of 3.4 minutes. Similarly, the effective breakthrough time of HFB is 15 minus 6.9 minutes, or 8.1 minutes. Using SF_6 as a reference, the measured retardation factor for HFB for this experiment is 8.1 divided by 3.4, or 2.4. Considering the uncertainty in the estimation of K_{oc} for HFB, the predicted retardation factor of 3.2 is in good agreement with the experimental value.

The large effect of temperature on the sorption of HFB on soil was demonstrated during the experiment with air-dry Yolo Loam (Figure 3.12). In this experiment, the temperatures of

the test gas in the extensions above and below the soil column were monitored continuously (the temperatures in the two extensions were the same within experimental uncertainty). As shown in the figure, there was an eight-hour time lag after introducing HFB to the column before any appreciable increase in the concentration of HFB was measured at the outlet. During this period, in which the normalized outlet concentration remained less than 0.1, the temperature of the test gas was steadily decreasing. As temperature decreases, the sorption coefficient and the total sorptive capacity of the soil increases. Had the experiment been conducted isothermally, the breakthrough time for HFB would certainly have been shorter. The reverse effect of temperature was observed at hour 13 when the temperature rose, and the concentration of HFB at the outlet increased to above the inlet concentration. This effect was further demonstrated during the transport of HFB across air-dry Panoche Soil (not shown). When the outlet concentration had reached a steady state, the soil column was rapidly heated with a heat gun. Almost instantaneously, the outlet concentration rose to well above the inlet concentration. These results indicate that lack of temperature control in the experiments could account for the longer breakthrough time of HFB in Yolo Loam than in Panoche Soil even though the clay content of Panoche Soil is higher.

The relative magnitude of the retardation of HFB in Delhi Sand versus the retardations in Yolo Loam and Panoche Soil is not readily explained. The retardation in Delhi sand is approximately a factor of ten less than the retardation in the other two soils, yet the clay content of Delhi Sand is relatively close to that of Yolo Loam. A more detailed understanding of the effects of soil parameters on retardation would require further experimentation using a temperature controlled system and soils with a wider range of particle-size distributions and organic-carbon contents.

CONCLUSIONS

The soil-column apparatus and method proved to be suitable for evaluating the behavior of tracer gases proposed for use in the field. The breakthrough times of SF_6 and HFB in

three soils at two conditions of soil moisture were measured and compared. The SF_6 tracer gas was not sorbed by any of the soils. The flow of HFB tracer gas was always retarded relative to the flow of SF_6, and HFB was strongly sorbed by two air-dry soils. The measured and predicted retardation factors for HFB in a wetted soil, more typical of soils in the natural environment, had a value of approximately three. Based on these results, SF_6 appears to be a good tracer gas for use in the field to measure the advective flow of soil gas, at least over the relatively short distances applicable to the investigation of soil-gas entry into houses. Because HFB is sorbed onto the soil, its behavior in soil may be similar to that of other VOC. Comparisons with VOC of interest could be made with this apparatus and method (modified for temperature control). The major disadvantages of a tracer gas that is sorbed by soil are that considerable mass could be lost to the soil and its residence time in soil might be unacceptably long.

As stated above, this apparatus and method are suitable for measuring the relative retardation factors, and hence the relative advective mobility, for VOC. For a more detailed understanding of the mechanisms of retardation and retention of VOC in soil, it is recommended that the solid-vapor phase transfer kinetics of VOC be investigated. If the transfer kinetics for these compounds are found to be rapid, then soil-column experiments can provide a measure of the soil-sorption coefficient (Equation 2.11).

Because of the lack of good soil-sorption data for VOC, and the uncertainty of the data regressions used for the calculation of the sorption coefficient, it is recommended that more sorption isotherms be measured for these compounds and the results be compared with the existing data regression (Equation 2.8). These sorption data could then be used in conjunction with soil-column experiments to test the model for pressure-driven transport (Equation 2.14).

CHAPTER 4

TRANSPORT OF VOLATILE ORGANIC COMPOUNDS FROM SOIL INTO A RESIDENTIAL BASEMENT

INTRODUCTION

The primary objective of this phase of the investigation was to assess the importance of pressure-driven flow of soil gas in the entry of volatile organic compounds (VOC) into a house with a basement adjacent to a municipal landfill. The study consisted of two interrelated components. In the first, the physical mechanisms of soil-gas entry were investigated using two techniques: 1) measurement of the pressure field developed in the soil around the house while the basement was depressurized with an exhaust fan, and 2) monitoring of the movement of a tracer gas from the soil into the basement with depressurization. Contamination of the soil gas and indoor-air quality were examined in the second component by means of measurements of VOC in soil gas, outdoor air and indoor air.

METHODS

Description of Study Site

The study site was an unoccupied, single-family residence in Central California located adjacent to a covered municipal landfill. There was previous evidence of migration of landfill gas and VOC from the landfill to the site. In 1983, the county, which operates the landfill, installed air-injection pumps at the perimeter of the landfill to contain methane which was detected at this house and other nearby residences. Samples of well water collected by several agencies at the site from 1985 through 1986 were found to contain Freon-12, Freon-11, tetrachloroethylene, and other halogenated compounds.

The residence was constructed in 1977 after the landfill had begun operation. It is a three-bedroom, one-story structure built over a garage and a basement which is below grade. The

foundation and basement of the house were constructed by excavating the soil, pouring a cement slab and building up a cement-block wall on top of the slab. The cavities in the wall were backfilled with cement, and the exterior of the wall was sealed with an asphalt-based product. The interior of the wall and the floor were painted. The areas of the first floor and the basement are 183 and 103 m^2, respectively. A plan view of the house and site is shown in Figure 4.1. The berm containing the landfill is approximately 70 m to the west of the house at its closest point. The land between the berm and the house is flat and covered with grass. The land immediately to the east of the house slopes steeply downward for a vertical drop of approximately 10 m. The prevailing wind during the study was from the direction of the landfill.

Investigations at the site were conducted over a period of about four months from late July through early November, 1987. Thus, the study was largely conducted during the hot, dry summer season. There was only 1.5 cm of rainfall which occurred in the last two weeks of October. Rainfall during the preceding winter was low.

Characterization of Soil.

The USDA soil type was determined by standard sieving and hygrometer-technique sedimentation analysis for particle-size distribution (Day, 1965). The eighteen soil samples collected for analysis were extracted by bucket auger from three vertical profiles located 0.8, 4.3 and 10.7 m from the west basement wall. Sampling depths ranged between 0.3 and 2.8 m. The samples were sealed in moisture proof containers at the time of collection and were refrigerated within six hours. The moisture content of the samples was determined by weighing subsamples before and after drying to constant weight at $110^{o}C$.

Three soil types were identified, sandy loam, loamy sand, and silt loam. The sixteen samples taken from above 2.3 m depth were sandy loams and loamy sands, having sand contents greater than 67 weight percent and clay contents below 10 weight percent. The two

samples from below 2.4 m depth were of the distinctly different type, silt loam, having more than 50 percent silt and less than 42 percent sand. This finding supported evidence of a dense layer occurring between 2.4 m and 3 m depth suggested by increased resistance to soil drilling and probe installation in this region. Samples taken from the vertical profile 0.8 m distant from the basement wall were of a single soil type, loamy sand. Uniformity of soil type in this profile was expected since the profile was within the region that was backfilled after construction of the basement wall. The water content of the soil increased from approximately two to four percent by weight over a depth range of 0.5 to 2 m. The water content of the deep silt-loam layer was approximately 12 percent.

Soil permeability to air was measured at each of 32 soil probes using the in-situ technique described in Appendix A. The results of the permeability measurements are presented in Table I. The mean permeability at a depth of approximately 1.5 m is 2.5×10^{-12} m^2 with a range of $0.3\text{-}20 \times 10^{-12}$ m^2. The permeability at the three, 3-m deep probes is not appreciably different. Since the soil probes were terminated in soil layers of apparent higher permeability, based upon resistance to probe insertion, the calculated mean permeability may somewhat exceed the actual average permeability of the soil. The range of permeabilities measured at the site is in agreement with the particle-size composition of the soil described above. Nazaroff *et al.* (1986), for example, report that permeabilities for uniform fine sands to uniform silts are typically in the range of 5×10^{-12} to 5×10^{-14} m^2. For comparison, the total range of soil permeability extends from 10^{-9} m^2 for coarse sands to 10^{-16} m^2 for homogeneous clay.

Construction and Installation of Soil Probes

Soil probes were installed at the site and were used in experiments to determine in-situ permeability of the soil, pressure coupling between the basement and the soil, soil-gas entry into the basement, and concentrations of VOC in soil gas. Thirty probes were installed around the house at distances ranging from 0.5 to 12 m from the basement wall and at depths ranging

between 1 and 3 m (Figure 4.1). The majority of these probes terminated at a depth of 1.5 m and were located to the west of the house between the house and the landfill. No probes were installed to the south of the house which was distant from the basement. Two probes were installed through the basement floor to a depth of 3.2 m below the grade level of the soil.

The soil probes consisted of 2- or 3-m lengths of 13-mm OD, 9-mm ID galvanized steel pipe open at both ends with the outlet end threaded to accommodate pipe-to-tube connectors. A guide hole was drilled in the soil prior to installation of a probe in order to minimize disturbance of the soil. A stainless-steel rod was inserted into the probe so that it extended 1 cm beyond the inlet end. The pair was then driven into the soil to the desired depth using a sledge hammer. After installation, the center rod was removed, and the inlet was augered to break up compacted soil. During both drilling and hammering, distinct soil layers offering greater or less resistance were detected. Probes were generally terminated in a relatively low resistance, presumably more permeable, layer. Soil probes were capped at the outlet when not in use.

Measurement of Pressure Coupling

Pressure coupling between the basement and the soil was determined using the technique of Nazaroff *et al.* (1987). A large exhaust fan (blower door), typically used to make leakage-area measurements in houses, was installed in the doorway between the basement and the garage (Figure 4.1). With the garage door open, the door between the basement and the upper floor closed, and the windows and doors on the upper floor open, the fan was operated to achieve a basement depressurization with respect to outdoor air of -25 Pa. This pressure was measured with a diaphragm differential-pressure gauge (0-60 Pa) and was maintained to within 2 Pa. With the basement at the desired pressure, differential pressures with respect to outdoor air were measured in the soil probes using a variable reluctance pressure transducer (Model DP103, Validyne Instr., Inc.). The pressure transducer was calibrated in the field and was periodically checked during use with a micromanometer.

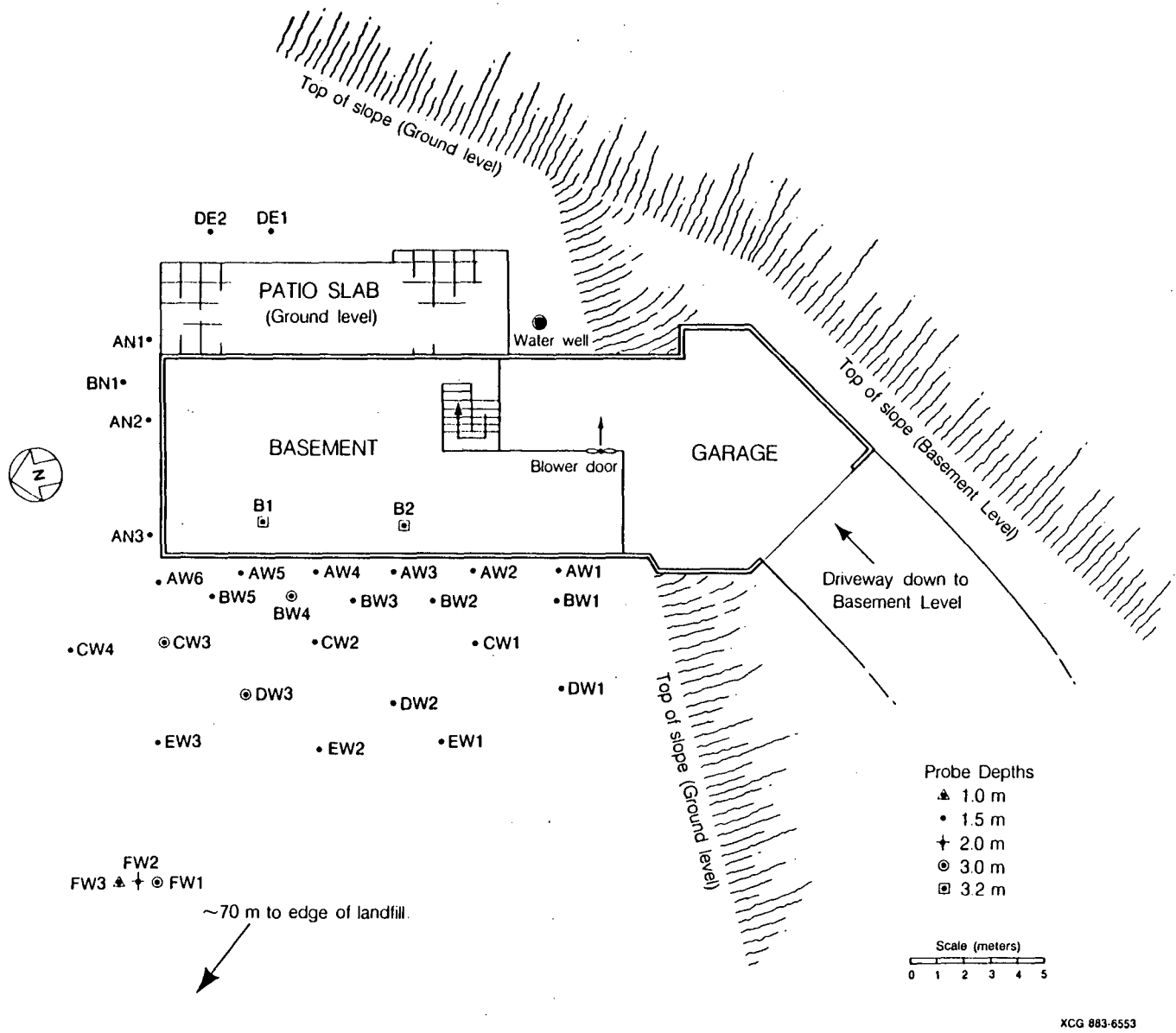

Figure 4.1 Plan view of the study site and the basement level of the house showing the locations and depths of the soil probes.

Estimation of Soil-gas Entry into the Basement

An experiment was conducted to estimate the entry rate of soil gas into the basement as a function of basement depressurization. The purpose of this experiment was to obtain an order-of-magnitude estimate of pressure-driven inflow of soil gas under typical operating and environmental conditions. Pure sulfur hexafluoride (SF_6) was injected into the soil around the house to provide a source of labeled soil gas. In September, a total of 490 cm^3 of SF_6 was injected into five soil probes to the north and west of the house (probes AN2, AW2, BW3, BW4, and BW5) in approximately equal portions. The experiment was conducted one month later in October after the SF_6 had diffused over most of the soil-probe field.

Shortly before beginning the experiment, duplicate samples of soil gas were collected from each probe using plastic syringes. The concentrations of SF_6 and Freon-12, a soil-gas contaminant present at the site at relatively high concentrations, were measured with an on-site, transportable gas chromatograph (GC) (Model 1030A, Baseline Industries, Inc.) equipped with an electron capture detector (ECD), a gas sampling loop and valve, and a molecular sieve (5A) column. Before the samples were collected, a volume of air equal to two probe volumes was withdrawn from the probe and discarded.

Meanwhile, the basement was thoroughly ventilated by running the exhaust fan at high speed for an extended period with the interior door to the upper floor and all windows and doors on the upper floor open. Then the door to the upper floor and all of the heating ducts in the basement were closed, and the GC-ECD was set up to automatically sample and analyze basement air for SF_6 and Freon-12 at one-minute intervals. The exhaust fan was operated to produce pressures in the basement of -20, -30, -40, and -50 Pa relative to ambient pressure. Each stage of depressurization was maintained long enough to achieve near steady-state conditions.

Sampling and Analysis of VOC

Samples of soil gas, outdoor air, and indoor air for qualitative and quantitative analysis of VOC were collected and analyzed using previously described methods (Hodgson *et al.*, 1986; Hodgson and Girman, In press). Samples were collected on multisorbent samplers containing Tenax-TA, Ambersorb XE-340 and activated charcoal (Part No. ST-032, Envirochem, Inc.). Sampling flow rates were 113 cm^3 min^{-1} (20^oC, 760 torr). Flow rates were regulated with electronic mass-flow controllers placed between the samplers and a diaphragm vacuum pump. Sample volumes for soil gas, outdoor air and indoor air were typically 0.23, 5.6 and 2.5-5.6 L, respectively. Single samples were collected for qualitative analyses at each sampling location. For quantitative analyses, duplicate samples were collected. Before samples of soil gas were collected from a soil probe, a volume of air equal to two probe volumes was withdrawn and vented. Soil gas was then drawn through either one or two parallel, in-line samplers.

Samples for VOC were collected on three occasions during the study. A preliminary survey was conducted in July in which samples for qualitative analysis only were obtained from two soil probes, from outdoor air between the house and the landfill, and from basement air. In September, samples for both qualitative and quantitative analyses were collected. Qualitative samples were obtained from one soil probe, from outdoor air, and from basement air with the basement at ambient pressure and at a depressurization of -20 Pa relative to ambient pressure. Quantitative samples were collected from three soil probes, from outdoor air, and from basement air at ambient pressure. In the final sampling period in October, samples for quantitative analysis only were collected from four soil probes and from indoor air in both the basement and the upper floor of the house. Prior to this period, the house had been closed for four weeks with the door between the basement and the upper floor closed. Samples were collected immediately after entering the house and before significant ventilation due to opening and closing of doors had occurred.

For analysis, a sample is thermally desorbed from the sampler and introduced into a capillary GC with a UNACON Model 810A (Envirochem, Inc.) sample concentrating and inlet-

ting system. Sample components are resolved with a GC (5790A Series, Hewlett-Packard Co.) equipped with liquid nitrogen subambient cooling and a fused-silica capillary column (DB-1701, J & W Scientific, Inc.). The GC is connected via a direct capillary interface to a 5970B Series Mass Selective Detector (MSD) (Hewlett-Packard Co.). For qualitative analyses, the MSD is continuously scanned from m/z 33 to m/z 250. For quantitative analyses the MSD is operated to monitor multiple, individually selected mass ions.

RESULTS AND DISCUSSION

Pressure Coupling between the Basement and Soil

With the basement depressurized, a pressure field was propagated through the soil around the house and was measured at the soil probes. Pressures in the probes are presented in Table 4.1 as percentages of basement depressurization. Pressure coupling 0.5 m from the basement wall was typically 30-40 percent, and, as expected, there was a general decrease in pressure coupling with increasing distance from the basement wall. Significant pressure coupling, in excess of ten percent, was observed 7 to 12 m away from the house. Similar results were reported for a house situated in soil with a uniform permeability of approximately 6×10^{-11} m^2 in which pressure coupling of about eight percent was observed 5 m away from the house (Sextro *et al.*, 1987).

On a number of occasions during the experiment, the exhaust fan in the basement was abruptly switched on or off to verify that the underpressures measured at the probes resulted from the depressurization of the basement. In each case, the soil pressure reached equilibrium within seconds of turning the fan on or off. Soil depressurization was measured as a function of basement depressurization at probes AN3, BW4, and DE1. Figure 4.2 shows that the soil pressures at these locations were quite linear with the pressure in the basement. Pressures at probe AN3, only 0.5 m from the basement wall, were most strongly coupled. Within the

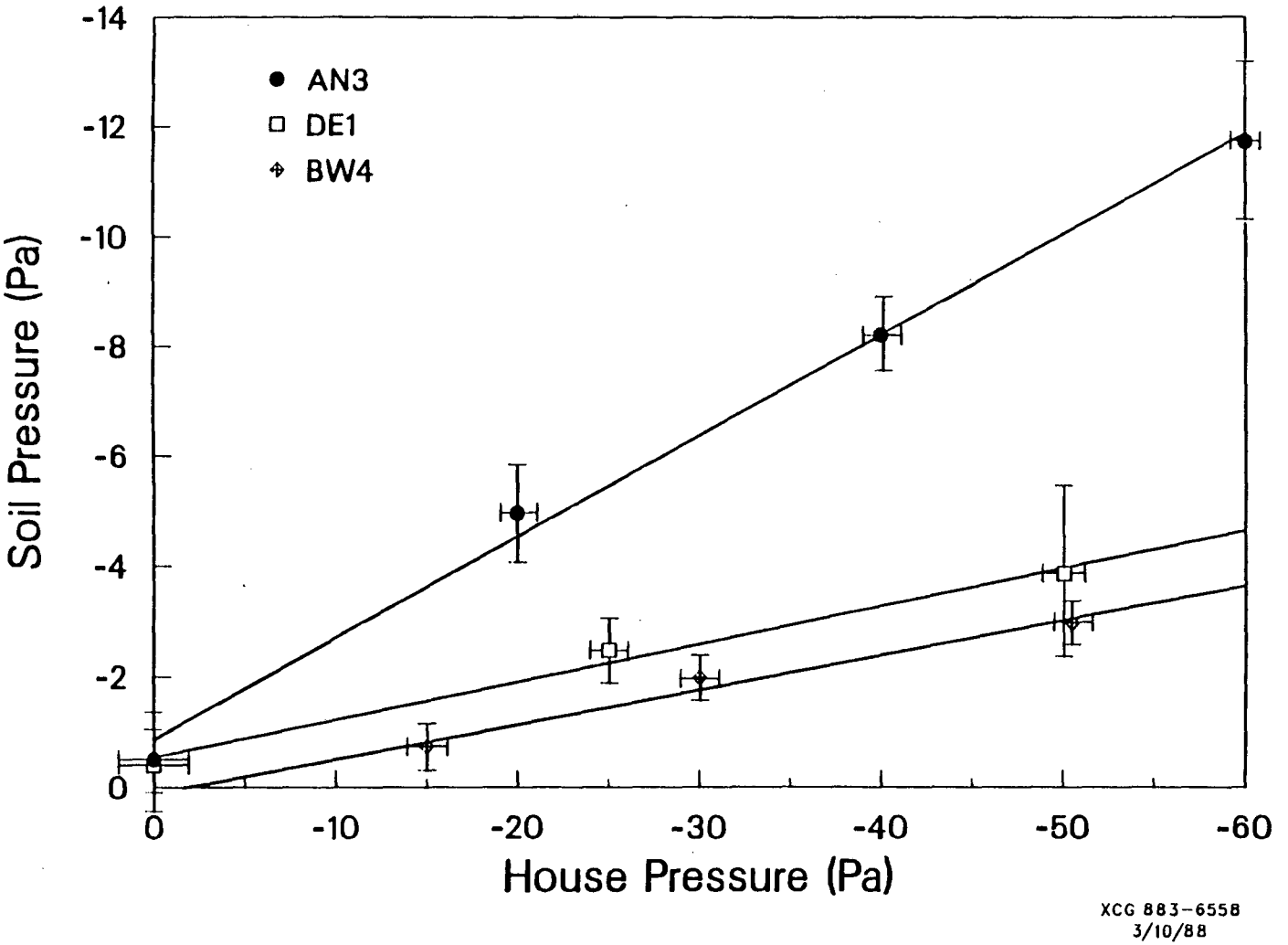

Figure 4.2 Depressurization of the soil as a function of basement depressurization at three soil probes. The error bars represent the uncertainties in the measurements due to instrumental noise. Linear regressions fitted to the data are shown as solid lines.

TABLE 4.1 Soil permeability and pressure coupling of soil gas with basement air at soil-probe locations.

Probe ID	Distance from House[a] (m)	Depth[a] (m)	Soil Permeability[b] (m^2)	Pressure Coupling[c] (%)
AW1	0.5	1.5	2.2×10^{-13}	30±6
AW2	0.5	1.5	2.1×10^{-12}	33±4
AW3	0.5	1.5	1.0×10^{-12}	37±6
AW4	0.5	1.5	4.9×10^{-13}	33±13
AW5	0.5	1.5	1.1×10^{-12}	27±6
AW6	0.5	1.5	2.6×10^{-12}	4±3
AN1	0.5	1.5	5.8×10^{-13}	44±6
AN2	0.5	1.5	5.3×10^{-13}	37±6
AN3	0.5	1.5	3.9×10^{-13}	23±4
BW1	1.5	1.5	1.1×10^{-12}	17±5
BW2	1.5	1.5	3.4×10^{-12}	17±3
BW3	1.5	1.5	4.2×10^{-12}	20±3
BW4	1.5	3	1.6×10^{-11}	6±1
BW5	1.5	1.5	2.0×10^{-13}	28±6
BN1	1.5	1.5	2.7×10^{-13}	25±6
CW1	3	1.5	9.3×10^{-13}	12±3
CW2	3	1.5	3.0×10^{-11}	14±3
CW3	3	3	3.8×10^{-12}	18±3
CW4	3	1.5	6.6×10^{-13}	14±4
DW1	5	1.5	1.5×10^{-12}	10±2
DW2	5	1.5	2.4×10^{-12}	9±2
DW3	5	3	2.7×10^{-13}	21±5
DE1	5	1.5	2.3×10^{-13}	10±7
DE2	5	1.5	3.9×10^{-13}	7±7
EW1	7	1.5	1.1×10^{-12}	7±2
EW2	7	1.5	2.6×10^{-13}	17±5
EW3	7	1.5	1.3×10^{-12}	10±3
FW1	12	3	1.9×10^{-13}	16±3
FW2	12	2	5.6×10^{-14}	-[d]
FW3	12	1	2.1×10^{-13}	-
B1	0	3.2	2.1×10^{-11}	-
B2	0	3.2	1.6×10^{-13}	-

a. Distances and depths are approximate

b. Uncertainty is x/÷2

c. As percent of basement depressurization of -25 Pa; uncertainty is based upon instrumental noise

d. No data

uncertainty in the measurements, the intercepts of the slopes incorporate the origin.

VOC in Soil Gas

The composition of VOC in soil gas that was sampled from several soil probes in July and September is shown in Table 4.2. A total of 26 individual compounds were identified in these samples. Identifications were determined using mass spectral data bases and were confirmed, in many cases, by analyses of standards. No attempt was made to analyze compounds with very low boiling points (most Freons and C_4-C_5 hydrocarbons) in July. There was no major qualitative difference in the composition of the other compounds between July and September. In general, halogenated and oxygenated compounds were the dominant classes, both in terms of the numbers of compounds detected and relative peak heights. Compounds with distinctly high peak heights were dichlorodifluoromethane (Freon-12), trichlorofluoromethane (Freon-11), 1,1,1-trichloroethane, tetrachloroethylene, 2-propanone (acetone), 4-methyl-3-penten-2-one (mesityl oxide), and 2-ethyl-1-hexanol.

The concentrations of 14 compounds which were measured by GC-MSD in soil gas collected at several probes in September and October are presented in Table 4.3. Both the ranges of concentrations and the mean concentrations are shown since there were large quantitative differences among the probes in each sampling period. The generally larger variations in September may have been due to the inclusion of data from a 3-m deep probe with data from two 1.5-m deep probes, while the four probes sampled in October were all 1.5-m deep. Nevertheless, even in October, concentrations of individual compounds generally ranged over a factor of three to five among the probes. There were also major differences in the concentrations of the compounds between the two sampling periods. In September, the dominant compounds were Freon-12, Freon-11, and tetrachloroethylene. These compounds still had relatively high concentrations in October, while the concentrations of five other compounds increased considerably from September to October. These compounds were dichloromethane, 2-propanone, hexanal, 2-methylbutane, and toluene. These changes occurred

TABLE 4.2 Composition of VOC in soil gas, indoor air and outdoor air in July and September. "X" = present; "XX" = very high concentration; "t" = trace concentration and "-" = not detected.

Compound	July			September			
	Soil-Gas[a]	Basement	Outdoor Air	Soil-Gas[b]	Basement Ambient	Basement -20 Pa	Outdoor Air
HALOGENATED							
Dichlorodifluoromethane	ND[c]	ND	ND	XX	X	X	t
Chlorodifluoromethane	ND	ND	ND	X	-	X	-
Dichlorotetrafluoroethane	ND	ND	ND	X	-	-	-
Trichlorofluoromethane	ND	ND	ND	XX	X	X	t
Trichlorotrifluoroethane	X	-	-	-	-	-	-
Dichloromethane	-	X	t	-	X	t	t
1,1,1-Trichloroethane	XX	X	X	X	X	X	t
Tetrachloroethylene	XX	-	t	XX	X	X	t
OXYGENATED							
2-Propanone	XX	X	X	X	X	X	X
2-Propanol	X	-	-	-	-	-	-
2.4-Dimethyl-2-pentanol	-	-	-	X	-	-	-
Acetic acid	-	X	t	X	X	X	X
Hexanal	X	t	-	X	X	X	-
4-Methyl-3-penten-2-one	XX	-	-	X	-	-	-
3-Methyl-3-penten-2-one	-	-	-	X	-	-	-
3-Heptanone	X	-	-	X	X	X	-
2-Heptanone	X	-	-	X	-	-	-
Heptanal	X	-	-	X	t	t	-
2-Butoxyethanol	X	-	-	-	-	-	-
6-Methyl-2-heptanone	X	-	-	X	-	-	-
2-Ethyl-1-hexanol	-	-	-	XX	-	-	-
Nonanal	X	-	-	-	-	X	-
Decanal	X	-	-	-	X	t	X

TABLE 4.2 (Continued)

Compound	July Soil-Gas[a]	July Basement	July Outdoor Air	September Soil-Gas[b]	September Basement Ambient	September Basement -20 Pa	September Outdoor Air
ALKANE AND CYCLOALKANE							
2-Methylpropane	ND	ND	ND	X	t	X	-
2-Methylbutane	ND	ND	ND	-	X	X	t
n-Hexane	-	-	t	-	X	t	-
Methylcyclopentane	-	-	t	-	X	t	-
n-Heptane	-	t	t	-	X	t	X
n-Decane	-	-	-	-	X	t	-
n-Undecane	-	-	-	-	X	-	-
AROMATIC							
Toluene	X	X	X	X	X	X	X
Ethylbenzene	-	-	t	-	X	X	-
1,3- 1,4-Dimethylbenzene	-	t	X	t	X	X	t
1,2-Dimethylbenzene	-	-	t	X	X	X	t
Trimethylbenzene	-	-	t	-	X	X	-
Trimethylbenzene	-	-	-	-	X	t	-
Trimethylbenzene	-	-	-	-	X	X	-

a. Soil probes CW3 and DW3

b. Soil probe CW2

c. No data

TABLE 4.3 Concentrations of VOC in soil gas, indoor air and outdoor air in September and October.

	Concentration, ppb							
	September				October			
	Soil Gas		Base-	Outdoor	Soil Gas		Base-	Bed-
Compound	Range	Mean[a]	ment	Air	Range	Mean[b]	ment	room
HALOGENATED								
Dichlorodifluoromethane	230-920	490	2.3	0.2	110-340	190	15	10
Trichlorofluoromethane	7.6-110	46	0.8	0.3	42-230	140	2.0	3.3
Dichloromethane			1.2	0.1	50-200	120	9.6	13
1,1,1-Trichloroethane	1.4-11	4.9	0.7	0.3	2.8-9.4	6.1	1.5	1.6
Tetrachloroethylene	23-150	70	0.7	0.1	26-79	56	2.0	1.9
OXYGENATED								
2-Propanone	16-27	20	12	4.9	90-370	250	200	38
Hexanal	3.3-7.9	6.1	1.0		37-52	42	3.7	4.8
4-Methyl-3-penten-2-one	0-10	3.4						
3-Heptanone	0-6.8	4.2	0.6		7.8-15	9.9		
ALKANE AND AROMATIC								
2-Methylbutane			5.2	0.3	14-74	36	11	12
Toluene	1.4-35	13	4.3	0.9	41-92	66	12	11
Ethylbenzene			0.6		2.8-3.7	3.3	2.0	1.8
1,3- 1,4-Dimethylbenzene	0-0.9	0.1	1.9		9.3-12	11	6.8	5.9
1,2-Dimethylbenzene	0.2-1.7	0.7	1.0		3.4-7.2	5.8	3.9	3.0

a. Soil probes AW2, CW2 and B2

b. Soil probes AW2, CW2, CE1 and CE2

over a period in which there was a general decrease in average ambient temperature and some precipitation (1.5 cm). However, these factors would not be expected to alter soil parameters at the sampling depth.

In October, Freon-12 was quantified at all probe locations by GC-ECD. Considerable spatial variability was observed. The average concentration of Freon-12 for the site is 630 ppb with concentrations in the individual probes ranging from 100 to 2100 ppb. Concentrations in the 1.5-m deep probes on the west side of the house average 250 ppb and are distinctly lower than concentrations in the other probes. The average concentration for the 3-m deep probes, including the basement probes, is 1500 ppb, and the average concentration for all probes (1.5-m deep) to the north and east of the house is 1000 ppb. Higher concentrations of Freon-12 on the north side of the house suggest that this area may be closest to the path of migration of landfill gas. The considerably higher concentrations at depth suggest the possible presence of a layer of soil of lower permeability lying between 1.5 and 3 m and limiting transport to the atmosphere.

Gas in the landfill adjacent to the study site was not analyzed, and, in general, there are few data on the composition of the minor constituents of landfill gas. Nevertheless, it is probable that many, if not all, of the dominant compounds in the soil gas around the house originated from the landfill.

Brookes and Young (1983) present a list with some quantitative data of compounds that were detected in soil gas at six landfills in Great Britain. More than 100 compounds encompassing all of the major classes of organic compounds were detected and either identified or partially classified. Thirteen of the compounds found in soil gas in the present study (Tables 4.1 and 4.2) appear in this list. In most cases their concentrations in the landfill gas were greater than several ppm. At one of the six landfills, oxygenated compounds, halogenated compounds and alkanes were the dominant classes both in terms of numbers of compounds and concentrations. Similarly, oxygenated and halogenated compounds are dominant in the present

study.

If conditions are favorable, VOC contained in landfills can be transported away from the site by subsurface water and by subsurface gas-phase migration. Gas-phase migration of VOC into surrounding areas was detected at two sites included in a survey of 20 nontoxic, municipal landfills in Southern California (Wood and Porter, 1987). At one location where methane was detected in nearby houses at concentrations approaching one percent, a sample of migrating gas was taken from a gas well outside the periphery of the landfill and another sample was taken from under the kitchen sink of a house approximately 180 m away. Tetrachloroethylene and 1,1,1-trichloroethane were detected at both locations. Concentrations at the entry point into the house were about two orders of magnitude lower than in the well. At another location, qualitative changes in the composition of soil gas with distance beyond the landfill perimeter were investigated. The first compounds to disappear with distance were the oxygenated compounds followed by the aromatic compounds, the other hydrocarbons and the polar halogenated compounds. Tetrachloroethylene, a dominant compound in the present study, was one of the most persistent compounds.

Entry of Soil Gas into the Basement

The concentrations of SF_6 and Freon-12 measured by GC-ECD in samples of soil gas collected from the soil probes closest to the house are summarized in Table 4.4. As indicated by the averages and ranges for soil probes on the two sides of the house, the spatial variability in the concentrations of both of these compounds was large. This variation occurred in an area of relatively uniform soil. An examination of all of the data for SF_6 revealed that concentrations predictably decreased with increasing distance from the points of injection. As shown in the table, concentrations of SF_6, 0.5 m from the basement wall, were somewhat higher on the west side of the house than on the north side. In contrast to SF_6, the concentrations of Freon-12 were higher on the north side of the house than on the west side by about a factor of four. For both compounds, the highest concentrations occurred in

TABLE 4.4 Concentrations of SF_6 and Freon-12 in soil probes adjacent to the basement. Probes to the North and West were ~0.5 m from the basement wall and ~1.5 m deep.

Probe Location	Concentration, ppb Mean	Range	No. of Probes
SF_6			
North	56	30-84	3
West	130	55-200	6
Basement	800	710-890	2
Freon-12			
North	1100	560-1700	3
West	270	160-450	6
Basement	2100		2

the two probes penetrating the basement floor.

After thorough ventilation, the concentrations of SF_6 and Freon-12 in the basement at the beginning of this experiment were 0 and 1 ppb, respectively. Volumes of air equivalent to 4.8, 3.0, 5.9, and 5.6 basement volumes were respectively exhausted from the basement at depressurizations of -20, -30, -40, and -50 Pa. Figure 4.3, which shows concentrations of SF_6 in the basement at -20 Pa as a function of time, demonstrates that near steady-state conditions were achieved within about one hour at this pressure. Concentrations of SF_6 and Freon-12 in air sampled in the open upper floor of the house and outdoors near the basement sill plate were 0 and 1 ppb, respectively.

Direct evidence of the entry of soil gas into the basement was obtained from the experiment. During depressurization, air flow into the basement was detected at the electrical outlet boxes which were recessed into cavities cut into the cement block wall approximately 45 cm above the floor. The average concentrations of SF_6 and Freon-12 in air samples collected from the cavities on the west wall were about 90 and 200 ppb, respectively. These concentrations are similar to the average concentrations measured in the adjacent soil outside the wall. Air flow into the basement was also detected at the sill plate running around three sides of the basement at a height of about 30 cm above the surface of the soil. This location may serve as a major entry pathway for outdoor air.

A simple mass-balance model assuming steady-state conditions was applied to the concentration data obtained at the end of each depressurization stage. Setting the mass flow of a tracer gas in the exhaust air equal to the mass flow of the gas in the air entering the basement gives:

$$C_\infty F_f = C_s F_s + C_o F_o. \qquad (4.1)$$

The C_∞ is the final concentration of the tracer gas in the basement at equilibrium, and C_s and C_o are the concentrations in the soil gas and the outside air, respectively. F_f is the fan

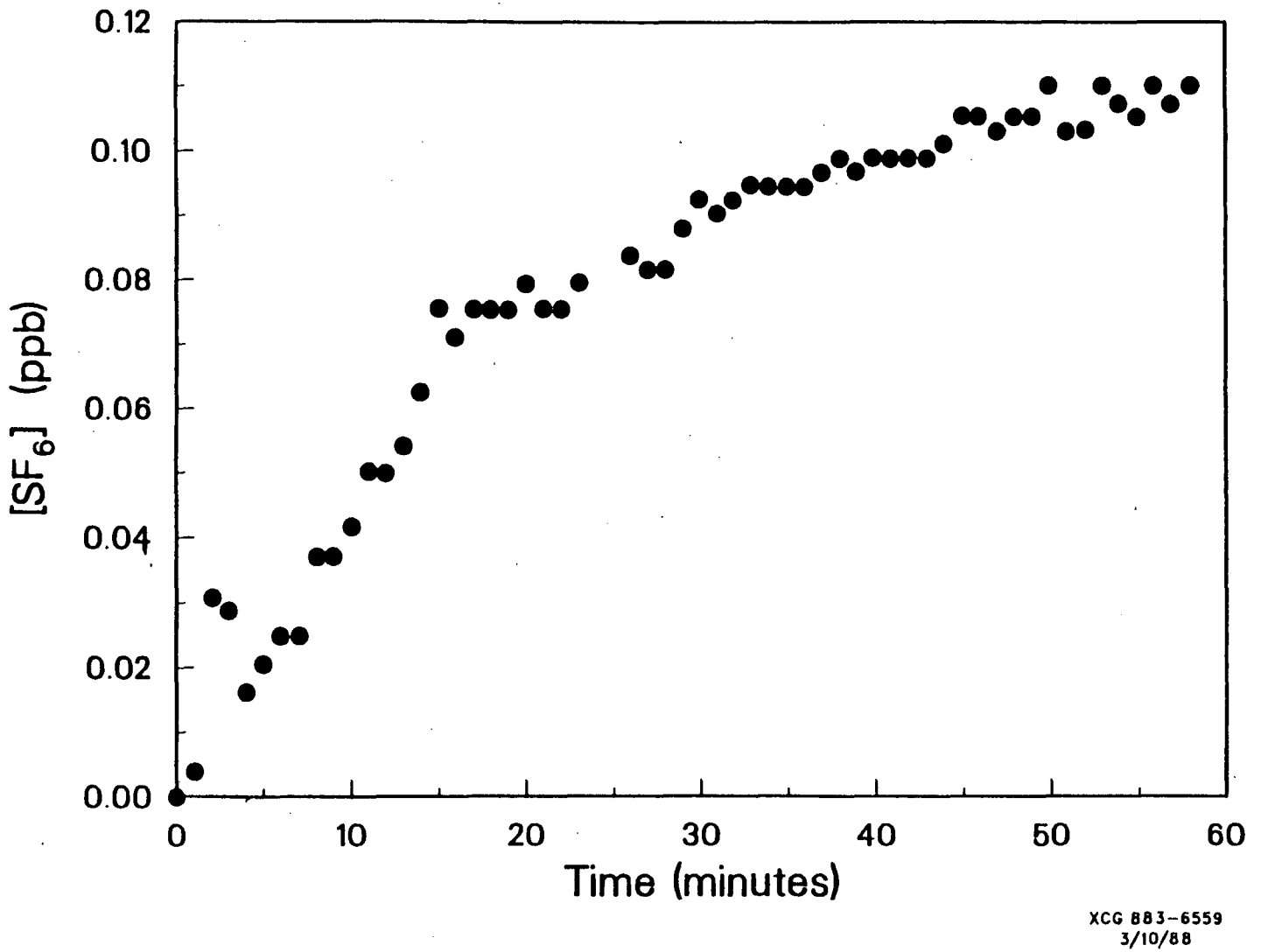

Figure 4.3 Concentrations of SF_6 tracer gas in the basement as a function of time with the basement at a depressurization of -20 Pa.

flow rate, and F_s and F_o are the flow of air from the soil and outdoors, respectively. (Outdoor air includes upstairs air in this experiment in which all upstairs windows and doors were open. The ventilation rate of the basement, a, is simply the calibrated flow rate of the exhaust fan. Solving for F_s, and letting $F_f = F_s + F_o$ yields:

$$F_s = a \frac{C_\infty - C_o}{C_s - C_o}. \qquad (4.2)$$

It was assumed that any soil gas entering the basement would be drawn from near the basement wall. Therefore, the averages of concentrations of SF_6 and Freon-12 in probes 0.5 m from the west and north walls and in the two basement probes were selected as the best estimates of concentrations for use in the mass-balance model. This results in values of C_s of 230 and 780 ppb for SF_6 and Freon-12, respectively. There is, however, considerable uncertainty in the estimates due to the large spatial variations which were observed (Table 4.4) and the lack of data for soil gas close to the east wall of the basement. As a result, the effective concentrations in soil gas entering the basement could vary from these values by a factor of two or more. The uncertainty due to spatial variations in concentrations is compounded by the fact that the distribution of the pathways for entry of soil gas into the basement is unknown. Together, these factors introduce considerable uncertainty into the estimation of entry rates.

The entry rates of soil gas into the basement as a function of basement depressurization which were estimated from the SF_6 and Freon-12 concentration data are shown in Figure 4.4. The relationship is linear for both compounds. The divergence between the two slopes, which is undoubtedly due to the large uncertainties discussed above, emphasizes the limitations of the experiment. Clearly, only order-of-magnitude estimates of entry rates of soil gas can be obtained by this method. However, despite the limitations, the regressions suggest that the entry rate of soil gas due to pressure-driven flow would be less than 1 $m^3\ h^{-1}$ at a basement depressurization of a few Pascals which would result from wind and an indoor-outdoor

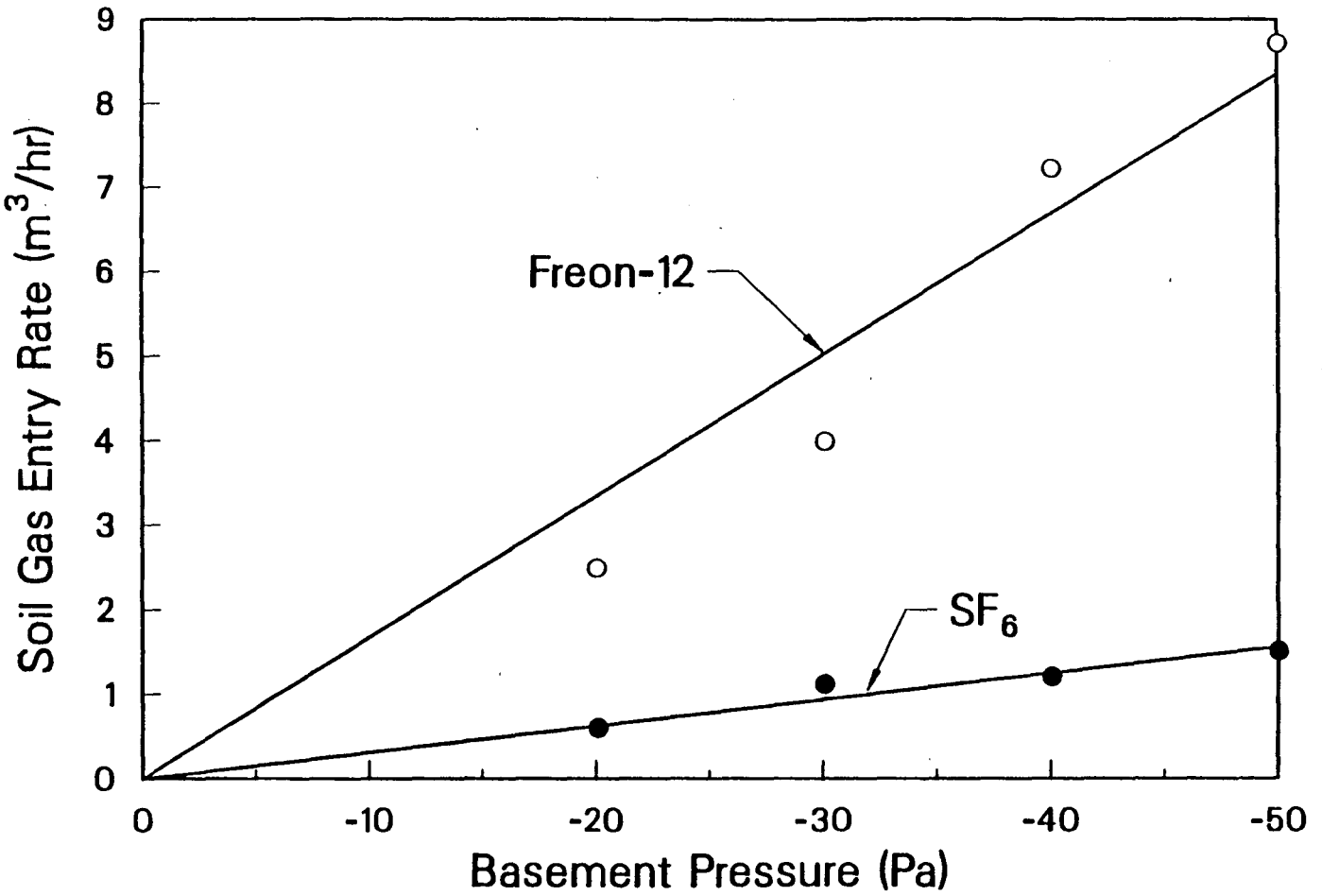

XCG 883-6564
3/15/88

Figure 4.4 Entry rates of soil gas into the basement as a function of basement depressurization estimated using a mass-balance model and concentrations of Freon-12 and SF_6 tracer gas in basement air, outdoor air, and soil gas adjacent to the house. Linear regressions fitted to the data are shown as solid lines.

temperature differential (Nazaroff *et al.*, 1988). For comparison, the infiltration rate of outdoor air for the whole house was calculated for relatively extreme winter conditions by the method of Sherman and Grimsrud (1980). Using the measured leakage area of the house and assuming a wind speed of 4 m sec^{-1} and an indoor-outdoor temperature differential of 22°C, this infiltration rate would be approximately 500 m^3 h^{-1}, or almost three orders of magnitude higher than the estimated soil-gas entry rate. For comparison, in a study of the basement-soil leakage characteristics of 14 houses, Turk *et al.* (1987) measured soil-gas entry rates between 0.4 and 39 m^3hr^{-1}, representing between one and 20 percent of total house infiltration.

The advective source term of Freon-12 (the concentration of Freon-12 times soil gas entry rate) was compared with estimates of the diffusive flux (Fickian flux ($D\nabla C$) times basement wall area) expected during normal house operation, where D is the diffusion coefficient of Freon-12 in the wall, and C is the concentration of the compound in the wall. The calculation was based on the concentrations of the compound measured in soil gas and basement air. Using: wall thickness = 0.2 m; wall area = 140 m^2; soil-gas concentration of Freon-12 = 5000 $\mu g\text{-}m^{-3}$; soil-gas entry rate = 0.3 m^3hr^{-1}, and; a diffusion coefficient in the wall ranging between 10^{-3} to 10^{-5} m^2hr^{-1}; the estimated advective source of 1500 $\mu g\text{-}hr^{-1}$ is bounded by the estimated diffusive source of between 3,000 and 30 $\mu g\text{-}hr^{-1}$. The upper limit on the diffusion coefficient was estimated based on the behavior of the diffusion coefficient of radon in concrete (D_{rc}) relative to that of radon in soil (D_{rs}), where $D_{rc}/D_{rs} \sim 10^{-3}$ (Nero and Nazaroff, 1984; Nazaroff *et al.*, 1988). The lower limit assumes the wall is at least 10 times more resistant to diffusive flux than soil. Since the estimated advective flux is bounded by the estimates of diffusive flux, it is not possible to rule out either source as a significant contributor to the entry of Freon-12 into this house. The relatively low concentration of Freon-12 observed in this basement is explained by the the relatively low contribution to basement infiltration of soil gas entry, as evidenced by the large visible infiltration observed at the above-grade sill.

VOC in Indoor Air

The compositions of VOC in the basement of the house in July and September are compared with compositions of VOC in outdoor air and soil gas in Table 4.2. For September, the compositions in the basement with the basement both at ambient pressure and at a depressurization of -20 Pa are presented. In July, only a few compounds were detected in the basement, and the composition is similar to that of outdoor air. Most of the oxygenated compounds present in soil gas did not appear indoors. In September, many more compounds were detected in the basement. Most of the halogenated compounds in soil gas appeared indoors, and more oxygenated compounds were detected indoors in this month. A number of alkane and aromatic compounds, e.g. n-hexane, methylcyclopentane, n-decane, n-undecane, and trimethylbenzenes, were detected only in the basement, suggesting indoor sources for these compounds. No significant increase in the number of compounds was observed when the basement was depressurized. However, seven of the compounds decreased to concentrations that were near their detection limits. This decrease was due to the dilution of basement air with infiltrating outdoor air.

The concentrations of VOC in the house in September and October are compared with concentrations in outdoor air and soil gas in Table 4.3. Thirteen of the 14 compounds quantified in soil gas appeared indoors, and eight of these were also present in outdoor air. In general, the concentrations of VOC in the house were very low, particularly in September when they typically ranged from less than one to a few parts per billion. In this month, acetone had the highest indoor and outdoor concentrations; Freon-12, which had very high concentrations in the soil gas, was not elevated in indoor air. Concentrations in outdoor air, with the exception of acetone, were all less than 1 ppb. Concentrations of VOC in the house in October were, with the exception of one compound, higher than they were in September by a factor of two or more. This increase may have been due to the additional care which was taken in October not to disturb the ventilation of the house prior to collecting samples. In this sampling period, concentrations of VOC in the basement were compared with concentrations in

a bedroom on the upper floor. The concentration of acetone in the basement approached the mean soil gas concentration which had increased considerably from September to October. The concentration of acetone in the bedroom was much lower suggesting that the source was in the basement. All of the other compounds had nearly equivalent concentrations in the basement and bedroom, with the possible exception of Freon-12 which was somewhat higher in the basement.

CONCLUSIONS

The measurement of significant pressure coupling at a distance of 12 m from the west side of the house demonstrates that soil gas can potentially be drawn by depressurization of the basement from a large area that extends out from the house toward the landfill. The significant pressure coupling that was measured on three sides of the house suggests that the pathway for the entry of soil gas into the basement is distributed around the house rather than located in one or in a few penetrations. The similarity of concentrations of tracer gas and Freon-12 in air coming from cavities on the inside of the cement-block wall when the exhaust fan was operating and in the adjacent soil outside the wall provided direct evidence of the entry of soil gas. However, the actual entry pathway for this soil gas is unknown.

The advective flow of soil gas into the basement of this house due to the pressure differential caused by wind and indoor-outdoor temperature differences is estimated to be only a small fraction, ~0.1 percent, of the inflow of air into the house due to infiltration, even at conditions of moderate wind and a relatively large temperature difference. Consequently, the infiltrating air would significantly dilute the concentrations of any contaminants entering from the soil. Although the basement is well coupled with the soil gas, the pressure-driven entry of soil gas, is limited by the relatively low permeability of the basement-soil membrane. In houses with higher leakage areas, situated in permeable soils, the relative contribution of pressure-driven inflow to total inflow can be much higher. Studies of radon entry into houses have shown that, in some cases, the fraction of soil-gas entry to the total infiltration rate can

approach 10-20 percent, or two orders of magnitude larger than observed for this house (Turk *et al.*, 1987).

The concentrations of Freon-12 and other VOC in soil gas were found to be highly variable in the vicinity of the house in an area of relatively uniform soil. It is probable that these variations arose from a combination of interrelated factors, such as the degree of coupling with the source, the presence of boundaries limiting transport to the surface, and differences in the sorptive capacity of the soil for VOC.

Some VOC, which were significantly elevated in soil gas relative to outdoor air, also occurred in indoor air at higher concentrations than in outdoor air, suggesting that the source of these compounds in indoor air was the soil gas. Entry of VOC into the basement of the study house is consistent with transport by either diffusion or convection. This result is explained by the relatively low permeability of the basement-soil membrane. In other houses with comparable pressure coupling and soil VOC, but higher basement-soil leakage area, advective flow of soil gas into substructures is certain to be an important mechanism for entry of VOC.

CHAPTER 5

PRESSURE FIELD MODELING

INTRODUCTION

In Chapter 4 an experiment was described in which pressure coupling between the basement of a house and the surrounding soil was measured during artificial basement depressurization. High pressure coupling, between 30 and 40 percent of the basement depressurization, was found at 1.5-m depth 0.5 m from the basement wall (Table 4.1). Pressure coupling on the west side of the house (where most of the measurements were made) was observed to decrease smoothly with increasing distance out to 5 m distance from the house. At distances greater than 5 m coupling showed a sudden increase. This was undoubtedly due to irregularity the large scale structure (macro-structure) of the soil, the increased coupling reflecting a zone of increased permeability between the basement and the far-field. Coupling greater than 10 percent was observed even at 12 m from the house, the farthest point at which measurements were made.

Various models have been developed for predicting pressure coupling between house basements and surrounding soil. These models have assumed homogeneous soil and a fixed basement leakage geometry. Loureiro (1987) developed a three-dimensional, finite-difference model for the simulation of radon entry into houses from soil gas. His model predicts the pressure field in order to determine the velocity field of the soil gas. Loureiro's model assumes that soil gas entry is confined to a crack at the basement wall-floor interface. For reasonable crack widths of 0.5 to 10 mm, the pressure coupling predicted is less than 10 percent at 1.5 m depth, 0.5 m from the basement wall. The predicted pressure field is fairly insensitive to changes in soil permeability. Mowris (1986) also numerically modeled pressure coupling between the basement and the soil while investigating the effect of exhaust ventilation on radon entry into houses. Like Loureiro, Mowris assumed homogeneous soil and a crack at the wall-floor interface. Mowris' model predicted pressure coupling of about 10-12

percent, 0.5 m from the wall, at 1.5 m depth, using crack widths between 1 and 10 mm. Coupling at 12 m from the house and 1.5 m depth was predicted to be less than 4 percent. Neither Loureiro nor Mowris compared the pressure field predictions with field data. Nazaroff *et al.* (1987) compare field data from a pressure-coupling experiment with pressures predicted from a simple analytical model. Based on the distribution of pressure coupling observed in the field, the authors assumed soil gas entry through a single penetration in the wall-floor joint. Their model predicted extremely low pressure coupling, 0.2 and 0.04 percent at 0.9-m depth, 2 m and 6 m from the house, respectively. The predicted values were more than a factor of 10 below the measured values. The authors hypothesized that the reason their theoretical predictions were low might have been due to layering of dissimilar soils which could not be included in the model.

In this chapter a two-dimensional finite element model (Sitar, 1985) is used as a tool to determine plausible mechanisms to explain the pressure coupling observed at the field site. The goal was to model the probe field to the west of the house, the area from which most of the pressure coupling data came. The model allows different permeabilities to be assigned to different elements, facilitating its use to study the effect of soil layering and various basement leakage geometries on the shape and extent of the pressure field. This flexibility makes the model an excellent tool for studying the sensitivity of the pressure field to various soil and basement permeability geometries - a considerable advantage over the previous models.

The modeling herein was not intended to simulate site conditions with high precision. That is, no serious attempt was made to determine in detail the macro-structure of the soil and incorporate it in the model. Rather, field measurements were used as indicators of the possible macro-structure. The model was then run with and without the indicated geometry in order to determine the magnitude of the effect on the pressure field.

MODEL DESCRIPTION

Originally designed to simulate groundwater flow, the finite element model used to predict the pressure field at the study site uses Darcy's Law as the governing equation (Equation 2.1). Since Darcy's Law is equally valid for groundwater or soil-gas flow, a simple scaling of the input flow-parameters rendered the model suitable for the present application. The program code is in Fortran and runs on an IBM-PC AT with a math coprocessor. To initialize the program, the user enters the components of a flow-net, which specifies the geometry of the site to be modeled. The flow-net divides the site area into elements which are defined by the cartesian coordinates of the nodes, or corners, of the element. Each element is assigned a permeability. The element size determines the resolution of the solution. The program solves Equation 2.1 across each element under the constraints imposed by the user-defined boundary conditions. Boundary conditions are assigned by designating boundary nodes as either points of constant pressure (such as the soil surface) or as points of flux with unspecified pressure (such at points in the porous media where the model is terminated but where, in reality, the media is continuous). Both of these designations represent boundaries across which there is fluid flow (flux boundaries). Boundary nodes not designated by either of these conditions are assumed to define a 'no-flow' boundary. The program generates a contour plot of the pressure field, and a digital listing of the pressure at each node and the fluid-fluxes at all flux boundaries.

As shown in the flow-net of Figure 5.1, the field site was modeled by taking an east-west cross-section at the mid-point of the basement. All of the flow-net boundaries were designated as flux boundaries, with the soil surface and the interior of the basement wall and floor designated as constant pressure boundaries. The flow-net was terminated 42 meters to the west of the house in order to minimize boundary effects in the region of the western probe field. The basement wall and floor were incorporated as elements in the flow-net and assigned a thickness of 0.25 m. Because of hardware memory limitations a flow-net with variable sized

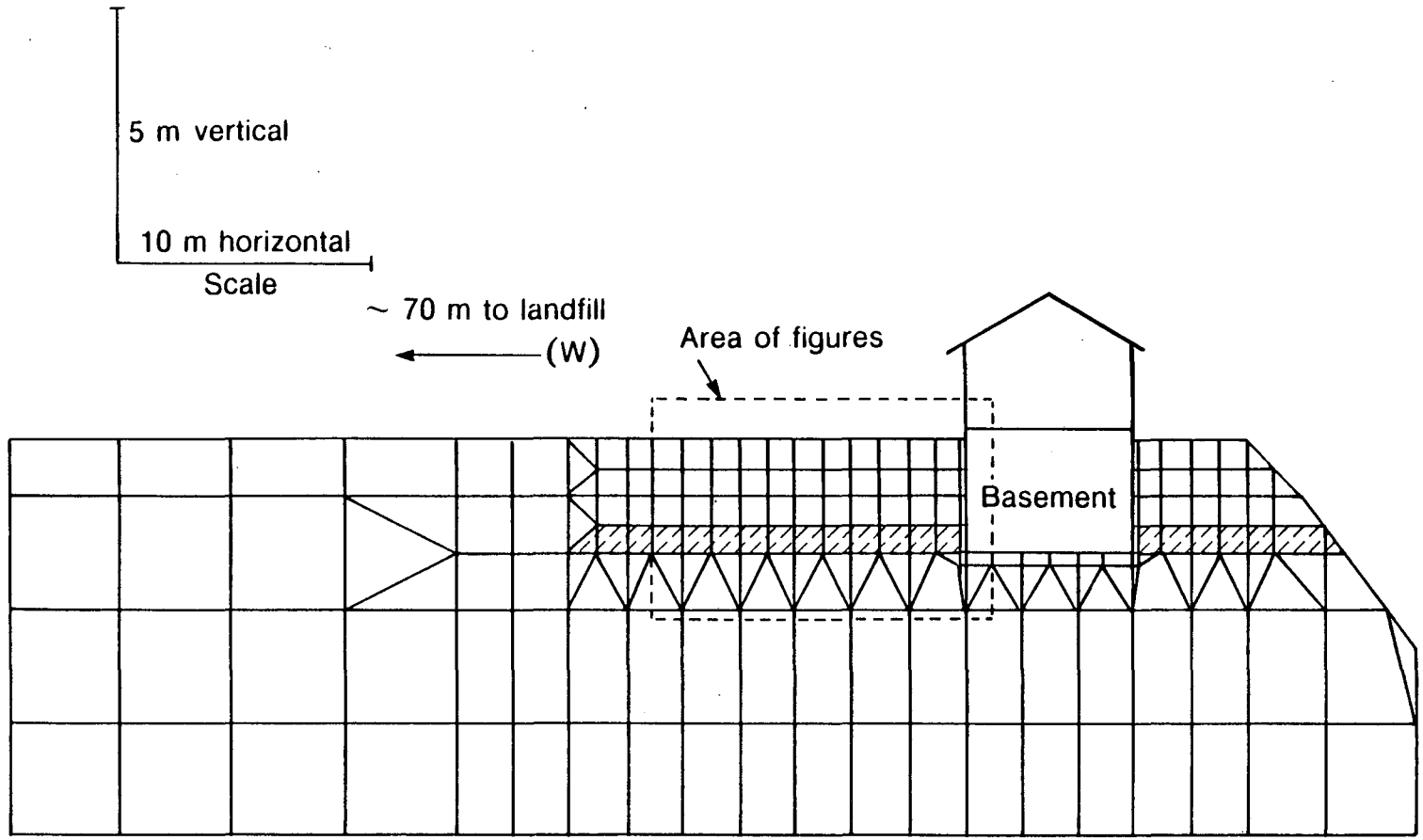

Figure 5.1. Flow-net for finite-element model showing basement and low permeability soil layer for model runs which did not incorporate the backfill zone.

elements was used. Fine mesh was used to define the basement walls and floor and in the probe field region where better resolution was required. Coarse mesh was used in outlying areas, thereby limited the total number of nodes and elements in the flow-net and reducing the computer data storage requirements. In all runs of the model the soil surface and basement interior were specified as constant-pressure boundaries at zero and -25 Pa respectively. The east and west sides and and lower boundary of the flow-net were specified as flux boundaries.

In order to simulate the effect of soil layering and basement leakage geometry on the pressure field, the permeabilities of the soil elements and the wall and floor elements of the basement were varied between model runs. Table 5.1 summarizes the permeabilities assigned to the soil, wall, and floor elements in each of the 14 runs of the model. The pressure field maps generated by the finite element program are shown for selected runs in Figure 5.2 to 5.9, and are listed in Table 5.1 for reference. In runs 1 through 7 the soil was treated as a homogeneous medium by assigning the average permeability measured at the site (3×10^{-12} m^2) to all soil elements. To simulate soil layering (model runs 8 through 14) the bulk of the soil was assigned the average permeability while the layer between 1.8 and 2.4 m was assigned a permeability of 3×10^{-14} m^2 (see Figure 5.1). This value was chosen based on results of the particle size distribution analysis (Chapter 4). The low permeability soil layer was terminated 17 m to the west of the house because at greater distances the elements of the flow-net were not fine enough to define the layer. Termination of this layer at this distance should not result in distortion of the pressure field within 5 m of the house, the area for which the model is compared with the data.

The layered-soil model was then modified to determine the effect on the pressure field of incorporating a backfill region next to the basement wall. This region is a result of backfilling the house excavation hole with soil after the completion of basement construction (Figures 5.8 and 5.9). The soil characteristics in the backfill region are therefore not expected to be the same as the surrounding soil. In runs 12 through 14, the backfill zone was taken to extend

Table 5.1 Permeabilities assigned to soil, wall, and floor elements in runs of finite-element model. (Permeabilities are 3 times the table values in units of m^2.)

Run no./ Fig. no.	MKdel ID S[a]	W[b]	C[c]	B[d]	Bulk soil	Layer soil	Wall	Floor	Crack
1/ 5.2	H	a	-	-	10^{-12}	10^{-12}	10^{-12}	10^{-20}	-
2	H	m	-	-	10^{-12}	10^{-12}	10^{-13}	10^{-20}	-
3	H	ml	-	-	10^{-12}	10^{-12}	10^{-14}	10^{-20}	-
4/ 5.3	H	l	-	-	10^{-12}	10^{-12}	10^{-15}	10^{-20}	-
5	H	vl	-	-	10^{-12}	10^{-12}	10^{-18}	10^{-20}	-
6/ 5.4	H	l	x	-	10^{-12}	10^{-12}	10^{-15}	10^{-15}	10^{-6}
7	H	vl	x	-	10^{-12}	10^{-12}	10^{-20}	10^{-20}	10^{-6}
8/ 5.5	L	a	-	-	10^{-12}	10^{-14}	10^{-12}	10^{-20}	-
9/ 5.6	L	l	-	-	10^{-12}	10^{-14}	10^{-15}	10^{-20}	-
10/5.7	L	l	x	-	10^{-12}	10^{-14}	10^{-15}	10^{-15}	10^{-6}
11	L	vl	x	-	10^{-12}	10^{-14}	10^{-20}	10^{-20}	10^{-6}
12/5.8	L	l	-	x	10^{-12}	10^{-14}	10^{-15}	10^{-20}	-
13/5.9	L	l	x	x	10^{-12}	10^{-14}	10^{-15}	10^{-15}	10^{-6}
14	L	vl	x	x	10^{-12}	10^{-14}	10^{-20}	10^{-20}	10^{-6}

a. Designation for soil model, either homogeneous (H) or layered (L).

b. Type of wall, either (a), (m), (ml), (l), or (vl), for average, medium, medium low, low, and very low permeability, respectively.

c. For model runs using the cracked wall geometry this column is x'd, for those which do not the designation is (-).

d. For models runs incorporating backfill in the soil layer this column is x'd, for models which do not the designation is (-).

from the basement wall out to 1.0 m and was assigned the average soil permeability. The low permeability soil layer then began 1.0 m from the house and extended, as before, out to 17 m on the west side of the house.

The wall and floor of the field house were backfilled cement block and poured cement, respectively. For the purpose of modeling these building materials were treated as homogeneous media with a given permeability. Two approaches were taken in modeling the basement wall and floor. The first assumed an impermeable floor (simulated by assigning floor elements an extremely low permeability of 3×10^{-20} m^2) with higher permeability walls. This type of model was used in runs 1 - 5, 8, 9, and 12, with wall permeabilities ranging from 3×10^{-12} m^2 to 3×10^{-18} m^2. The second approach essentially confined soil-gas entry into the basement to a 2 mm crack at the wall/floor interface. The crack was simulated by assigning a permeability of 3×10^{-6} m^2 (essentially infinite) to a 2 mm element at the floor level. The wall and floor were assigned the same permeability of 3×10^{-15} m^2 in runs 6, 10, and 13, and of 3×10^{-20} m^2 in runs 7, 11, and 14. Runs 1 and 8, in which the wall was assigned the average soil permeability, were used as reference cases. They were compared with runs using a lower permeability wall to facilitate understanding the effect of a low-leakage wall on the surrounding pressure field.

The crack geometry, suggested by Loureiro (1987) and Mowris (1986), applies best to a basement in which the floor slab is poured inside of a separate cement wall footer, resulting in slab shrinkage upon drying which can produce a peripheral crack. The basement of the house at which the field study was conducted was constructed by laying the concrete block wall on top of the slab. In this case slab shrinkage will not result in a crack. However, the difference in texture of the slab cement and the mortar used to build the cement block walls could result in some leakage at the interface. This effect is not expected to result in as large a leakage, however, as slab shrinkage, so we might not expect good agreement with the crack-geometry model. The model runs using the crack geometry were run: 1) for comparison with runs allowing soil gas entry through the entire wall area as a test of pressure field sensitivity to

basement leakage geometry; and 2) for comparison with the existing crack-geometry models of Loureiro (1987) and Mowris (1986).

RESULTS AND DISCUSSION

As stated in the opening paragraph of this chapter, pressure coupling data for probes at distances greater than 5 m from the house indicate an irregularity in the macro-structure of the soil. The two soil geometries modeled in this study, homogeneous and horizontal layering, will not predict such an irregularity. Therefore, the model predictions are compared only with data from the A, B, C, and D -ring probes, those lying between 0.5 and 5 m from the house. Table 5.2 presents the model predictions and the corresponding average probe pressures measured at 1.5-m depth. All values are presented as a percentage of the basement under-pressure.

A comparison of runs 1 through 5 demonstrates the effect of decreasing wall permeability on the near-house pressure coupling (compare A-ring values, Table 5.2). As expected, pressure coupling decreases with decreased wall permeability. In homogeneous soil, a reduction of wall permeability from 3×10^{-12} to 3×10^{-15} m^2 results in a reduction of predicted pressure coupling from 80 percent to 40 percent in the A-ring (runs 1-4). However, further decrease in wall permeability to 3×10^{-18} m^2 has little effect on the pressure field (runs 4 and 5). A comparison of runs 1 through 5 with the data indicates that, in homogeneous soil, even a wall permeability as low as 3×10^{-18} m^2 (two orders of magnitude lower than that of homogeneous clay) does not reduce the predicted coupling to the observed level.

The model runs with the cracked wall and homogeneous soil (runs 6 and 7) predicted A-ring coupling of 60 percent. Comparison of the pairs of cracked-wall models (6 and 7, 10 and 11, 13 and 14) provides further evidence that a reduction in wall (or floor) permeability beyond 3×10^{-15} m^2 has little effect on the pressure field. The crack model used in this

Table 5.2. Comparison of pressure coupling data and pressures predicted from the finite-element model. (All table values are percentage of basement depressurization.)

Run no.	Ring designation (distance from house) A(0.5)	B(1.5)	C(3.0)	D(5.0)
1/ 5.2	80	67	48	30
2	57	49	38	25
3	43	39	32	22
4/ 5.3	40	38	31	22
5	40	38	31	21
6/ 5.4	61	57	44	30
7	61	57	44	30
8/ 5.5	80	65	39	16
9/ 5.6	14	13	11	10
10/ 5.7	15	14	13	11
11	13	13	12	11
12/ 5.8	44	40	23	11
13/ 5.9	62	58	33	15
14	62	57	33	15
data[a]	32	21	12	10

a. Data values are the average pressure coupling of the 1.5 m deep probes in each ring.

study predicts significantly higher coupling than the models of Nazaroff, Loureiro, or Mowris. At 1.5 m from the house the present model predicts 61 percent coupling in homogeneous soil, whereas as the models of Nazaroff, Loureiro, and Mowris predict less than 10 percent coupling under similar conditions. A partial explanation could be the fact that the crack of the Loureiro and Mowris models penetrated the bottom of the building shell, whereas the crack of the present model penetrates the side of the shell, the different geometry reflecting different designs of the buildings being modeled.

Incorporating a low permeability soil layer has a dramatic effect on the pressure field. Figures 5.2 and 5.5, 5.3 and 5.6, and 5.4 and 5.7 show paired models, identical except for the inclusion or exclusion of the soil layer. As can be seen from the figures, a large pressure gradient develops across the low-permeability layer significantly decreasing pressure coupling at 1.5-m depth (above the layer). For example, including the soil layer in the low-permeability-wall model, runs 5.3 and 5.6, caused a reduction in the predicted coupling from 40 percent to 14 percent in the A-ring (Table 5.2). A visual comparison of the pressure fields generated by the homogeneous and layered soil models demonstrates that the net effect of the addition of the low-permeability layer is to propagate the pressure field to greater distances from the house while reducing coupling above the low-permeability layer. In other words, the presence of the layer reduces pressure coupling near the soil surface, but increases coupling with depth and distance.

An additional important effect of the presence of the low permeability soil layer is a reduction of dilution air entering through the soil surface. The direction of soil gas flow is always perpendicular to lines of constant pressure, and the permeability and the magnitude of the flow is determined by the magnitude of the pressure gradient. Therefore, comparing Figure 5.2 and 5.6, the influx of air from the atmosphere is clearly lowered by the presence of the soil layer, thereby reducing dilution of soil-gas contaminants entering the building and increasing indoor concentrations.

Incorporating the relatively high-permeability backfill elements in the low-permeability soil layer results in a large increase in predicted near-house coupling (out to 3 m), while far-field coupling is relatively unaffected. This effect is clearly seen by comparing the paired runs 9 and 12, 10 and 13, and 11 and 14. The members of each pair are identical except that the latter member incorporates the backfill zone. In effect, inclusion of the backfill zone makes the near-house pressure field resemble that of the homogeneous-soil model. Using a smaller backfill zone (it is not unreasonable to assume that the thickness of the backfill zone at full depth might be less than 1 m) would reduce near-house coupling, providing a better fit to the data.

CONCLUSIONS

The two-dimensional finite element model proved to be a useful tool for determining the effect of soil layering and basement leakage geometry on the pressure field and for exploring plausible mechanisms to explain the observed pressure coupling. The model's flexibility in the designation of different permeabilities for the flow-net elements is a great advantage over the models of Nazaroff, Loureiro, and Mowris. The present model predicted considerably higher coupling than the previous models in both the near and the far-field, providing better agreement with the field data. The pressure-field predicted by the present model was found to be considerably more sensitive to soil geometry than to the leakage geometry of the basement, with near-house pressure coupling more sensitive to model modifications than far-field coupling. The inclusion of a low-permeability soil layer was found to have a large effect on the predicted pressure field, the net effect being a reduction of near-surface pressure coupling, an increase in coupling with depth and distance from the house, and a decrease in dilution air entering the soil from the atmosphere. The presence of a soil layer, therefore, can increase the zone of influence of the house, determining the extent of the reservoir from which contaminated soil gas might be drawn.

The model results suggest that soil layering could be the most significant factor in

explaining the low observed near-house coupling at 1.5 m depth at reasonable wall permeabilities. Inclusion of the relatively high permeability backfill elements in the soil layer increased the predicted pressure coupling at 1.5 m to well above the observed level. Near-house coupling in closer agreement with the data would be predicted by using a smaller backfill zone in the model, or no backfill zone and a medium permeability wall. Since the low soil-gas entry rates estimated in Chapter 4 indicate a low wall permeability, the former is the more likely explanation of observed coupling at the field site.

In conclusion, groundwater models are readily available, flexible tools suitable for study of the pressure field generated in the unsaturated zone by basement depressurization. The modeling of the field site presented in this chapter indicates that the macro-structure of the soil around the basement is critical in the determination of the pressure field, which in turn will determine the avenue of soil gas entry to the house.

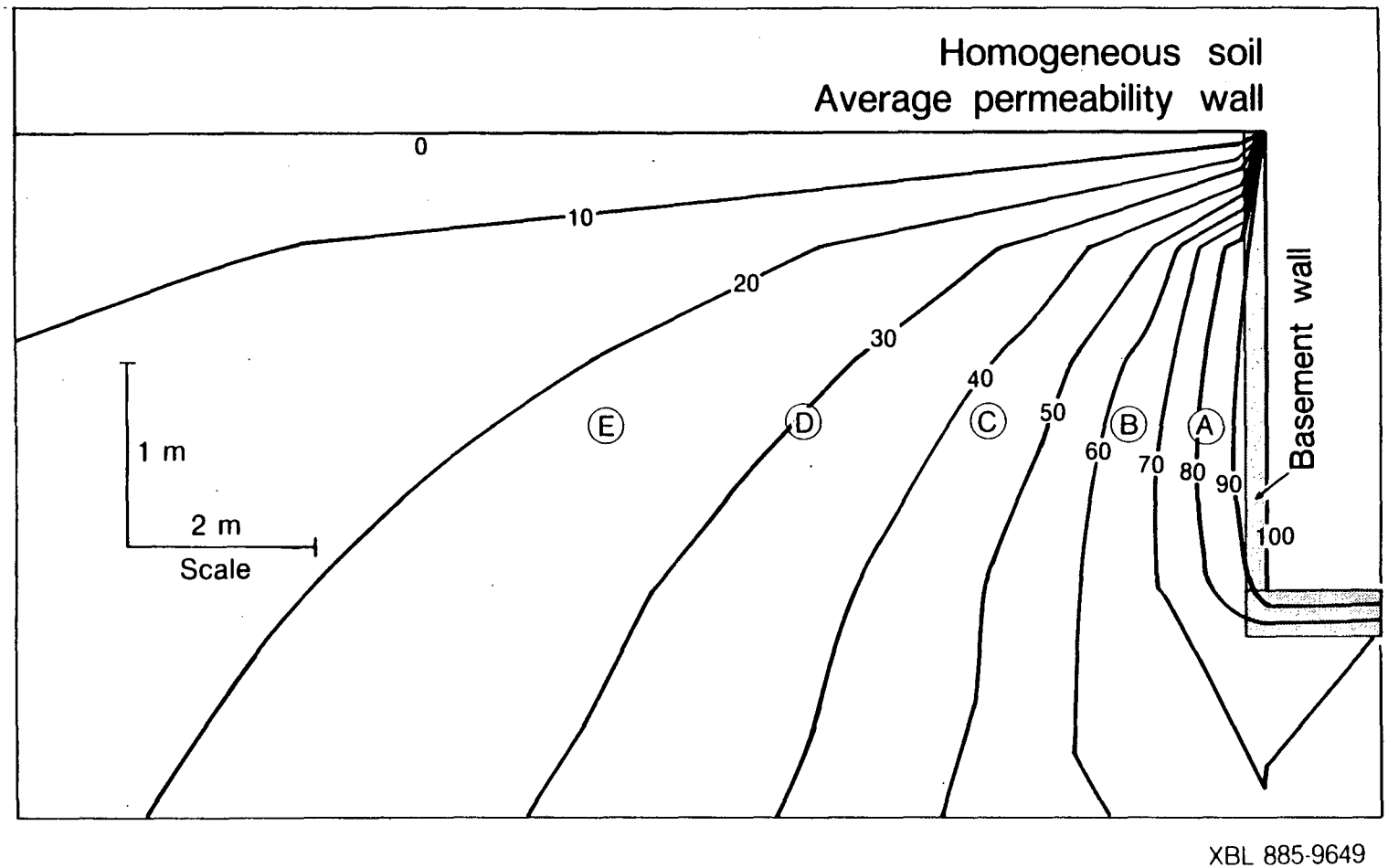

Figure 5.2. Pressure field generated by finite-element model using homogeneous soil and wall permeability equal to permeability of the bulk soil. Pressure contours are marked in percentage of basement underpressure. The zero percent contour is the soil surface. The circles lables (A - E) represent the probe locations.

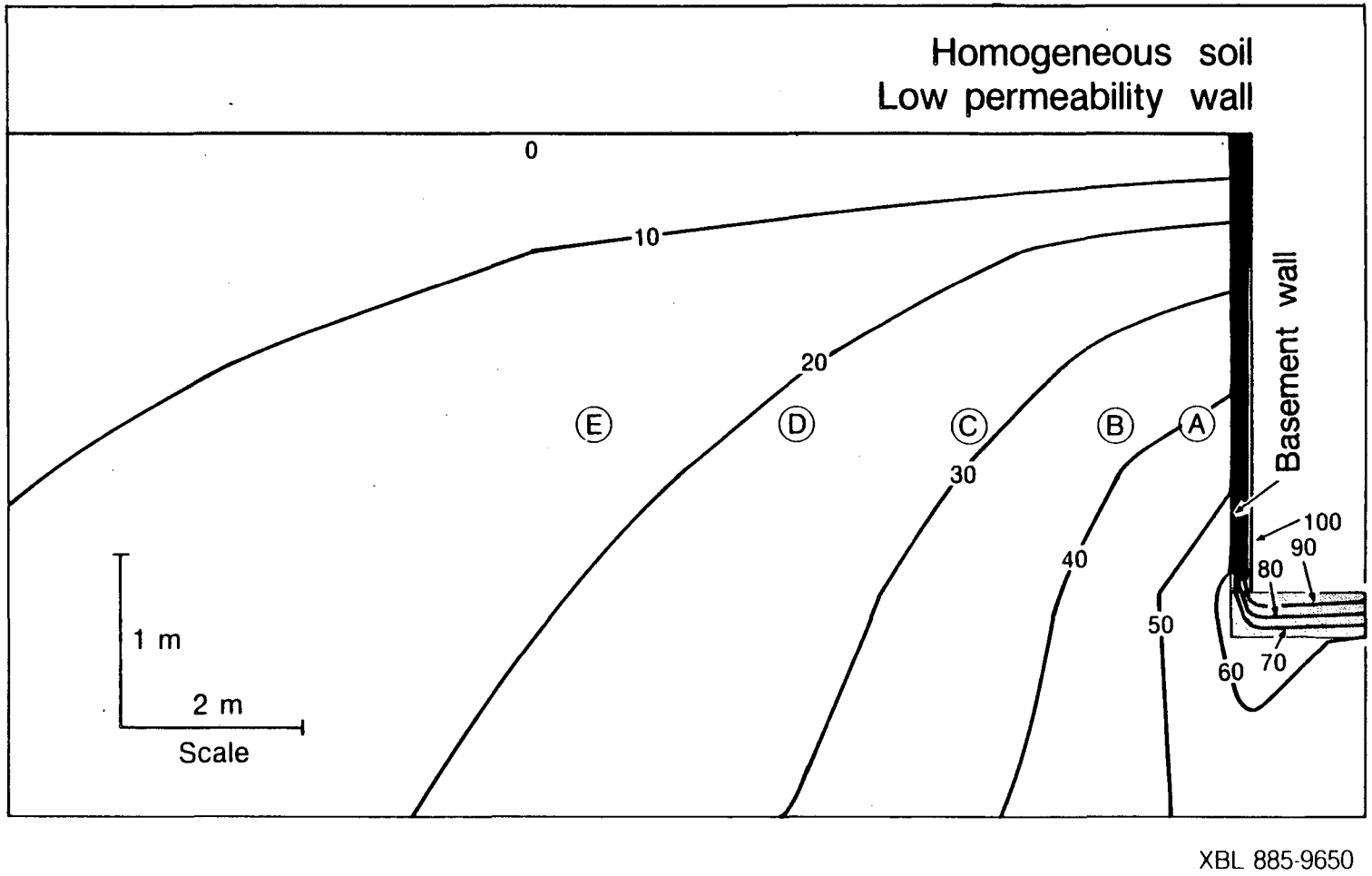

Figure 5.3. Pressure field generated by finite-element model using homogeneous soil and low permeability wall. Pressure contours are percentage of basement underpressure. The zero percent contour is the soil surface. The circles lables (A - E) represent the probe locations.

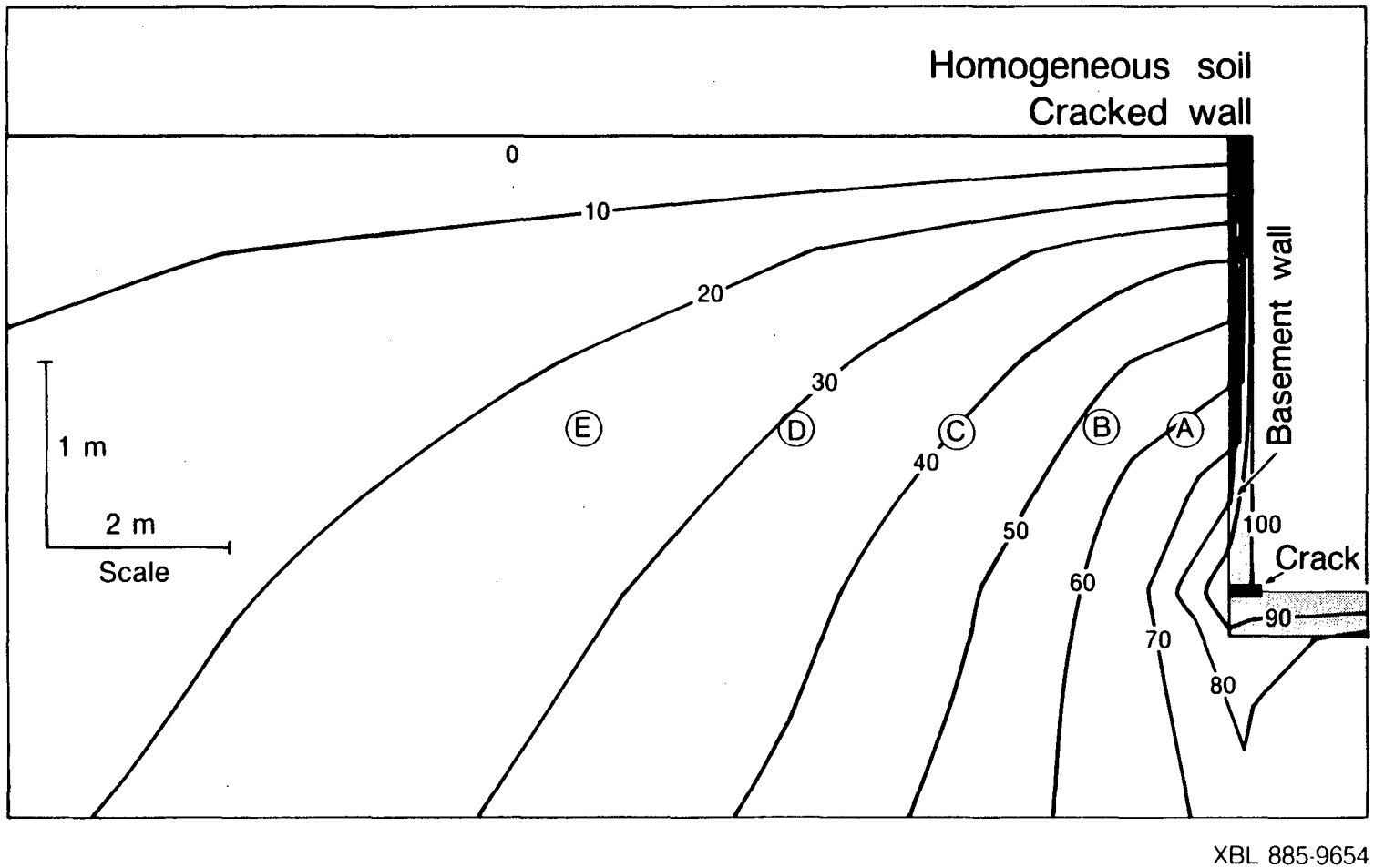

Figure 5.4. Pressure field generated by finite-element model using homogeneous soil and cracked wall geometry. Pressure contours are percentage of basement underpressure. The zero percent contour is the soil surface. The circles lables (A - E) represent the probe locations.

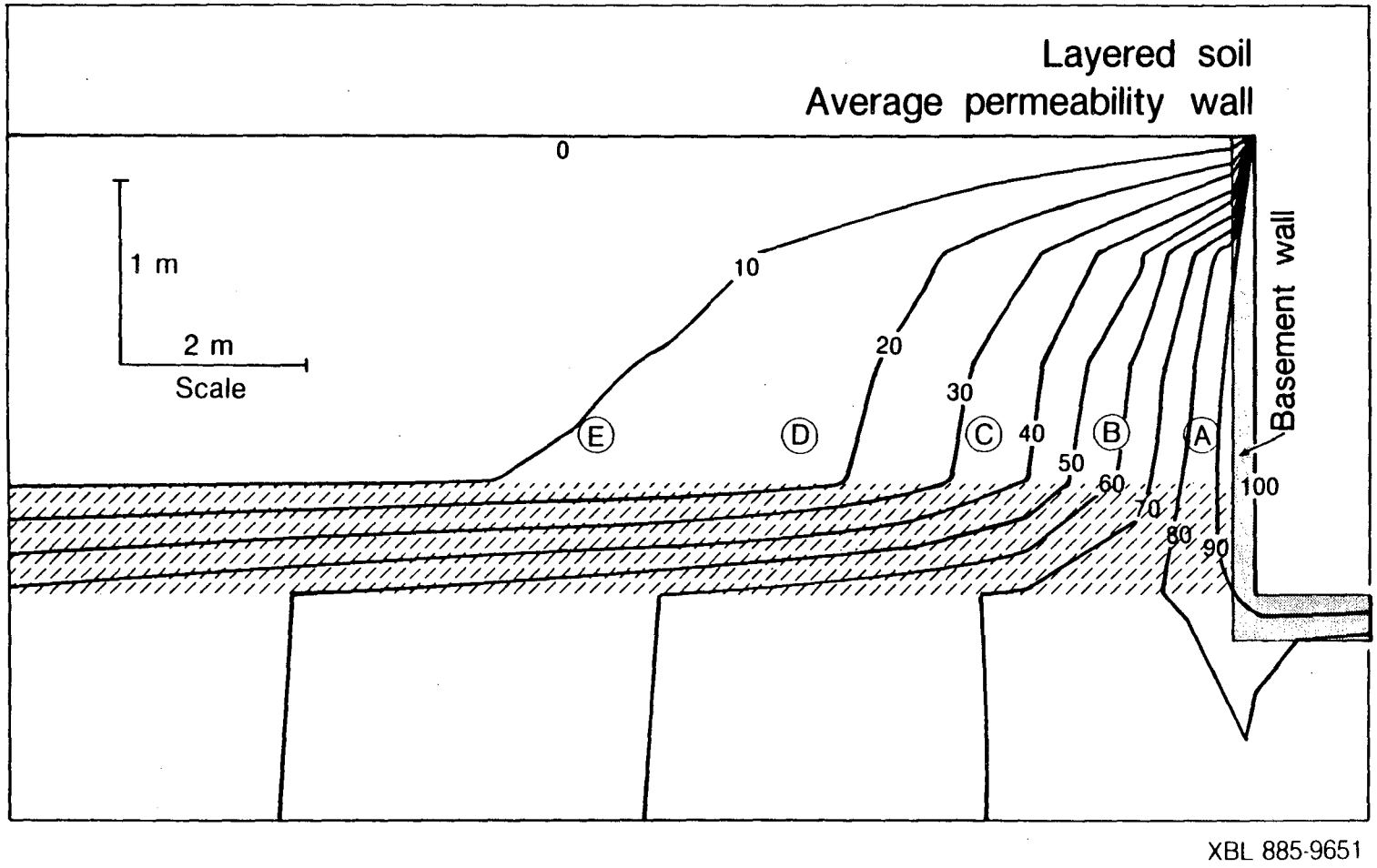

Figure 5.5. Pressure field generated by finite-element model using layered soil and wall permeability equal to permeability of the bulk soil. Pressure contours are percentage of basement underpressure. The zero percent contour is the soil surface. The low permeability soil layer is shaded, and the circles lables (A - E) represent the probe locations.

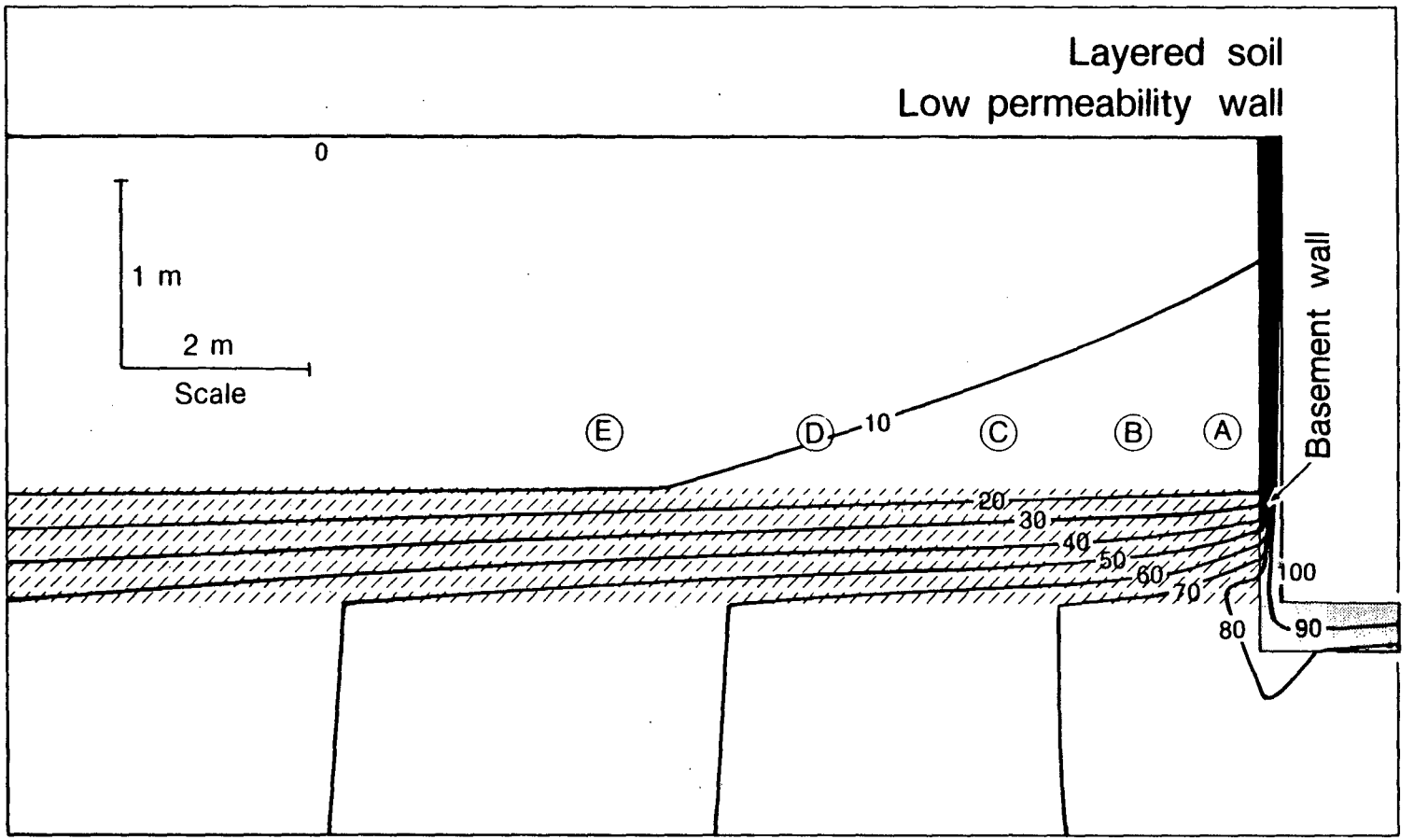

Figure 5.6. Pressure field generated by finite-element model using layered soil and low permeability wall. Pressure contours are percentage of basement underpressure. The zero percent contour is the soil surface. The low permeability soil layer is shaded, and the circles lables (A - E) represent the probe locations.

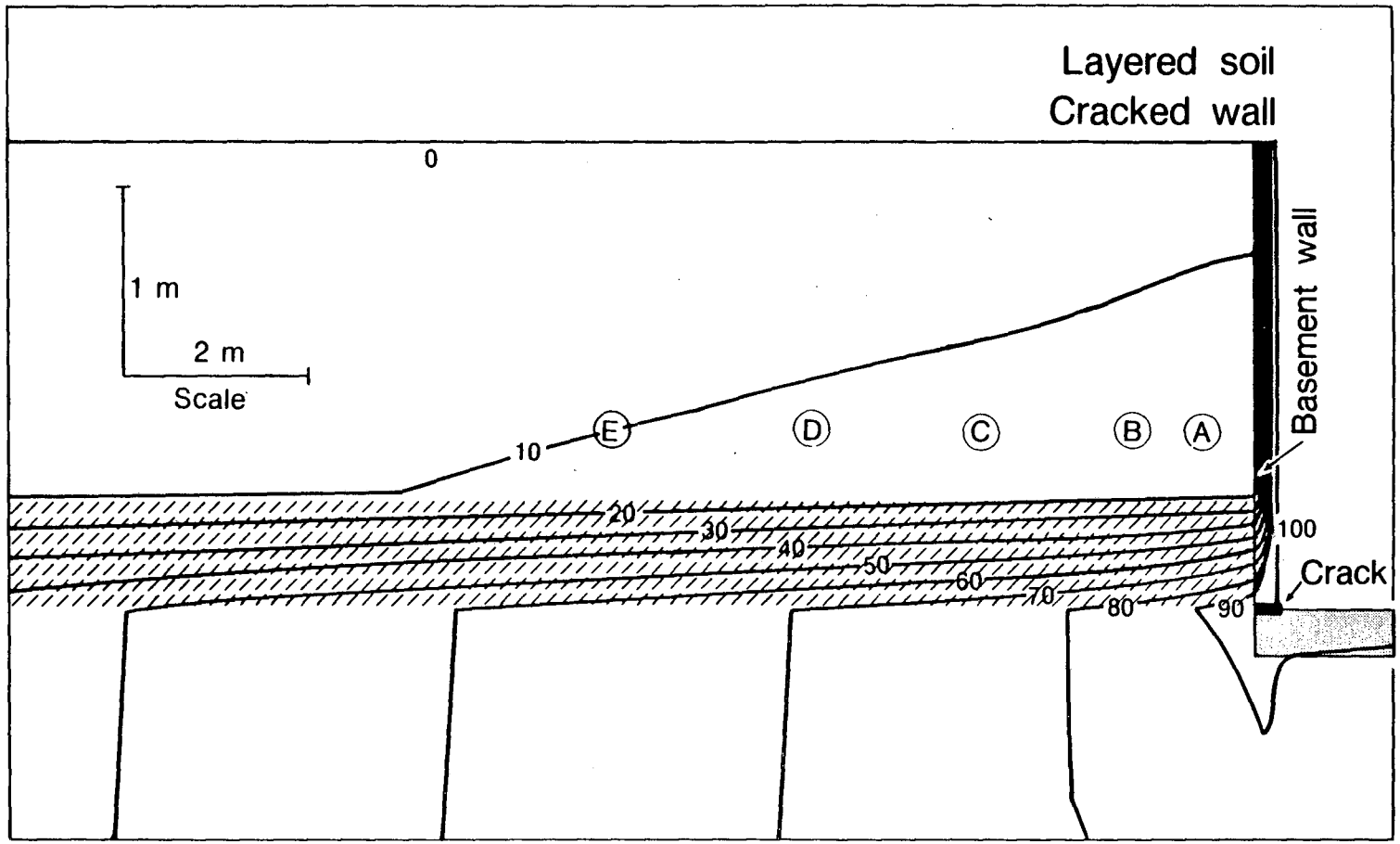

Figure 5.7. Pressure field generated by finite-element model using layered soil and cracked wall geometry. Pressure contours are percentage of basement underpressure. The zero percent contour is the soil surface. The low permeability soil layer is shaded, and the circles lables (A - E) represent the probe locations.

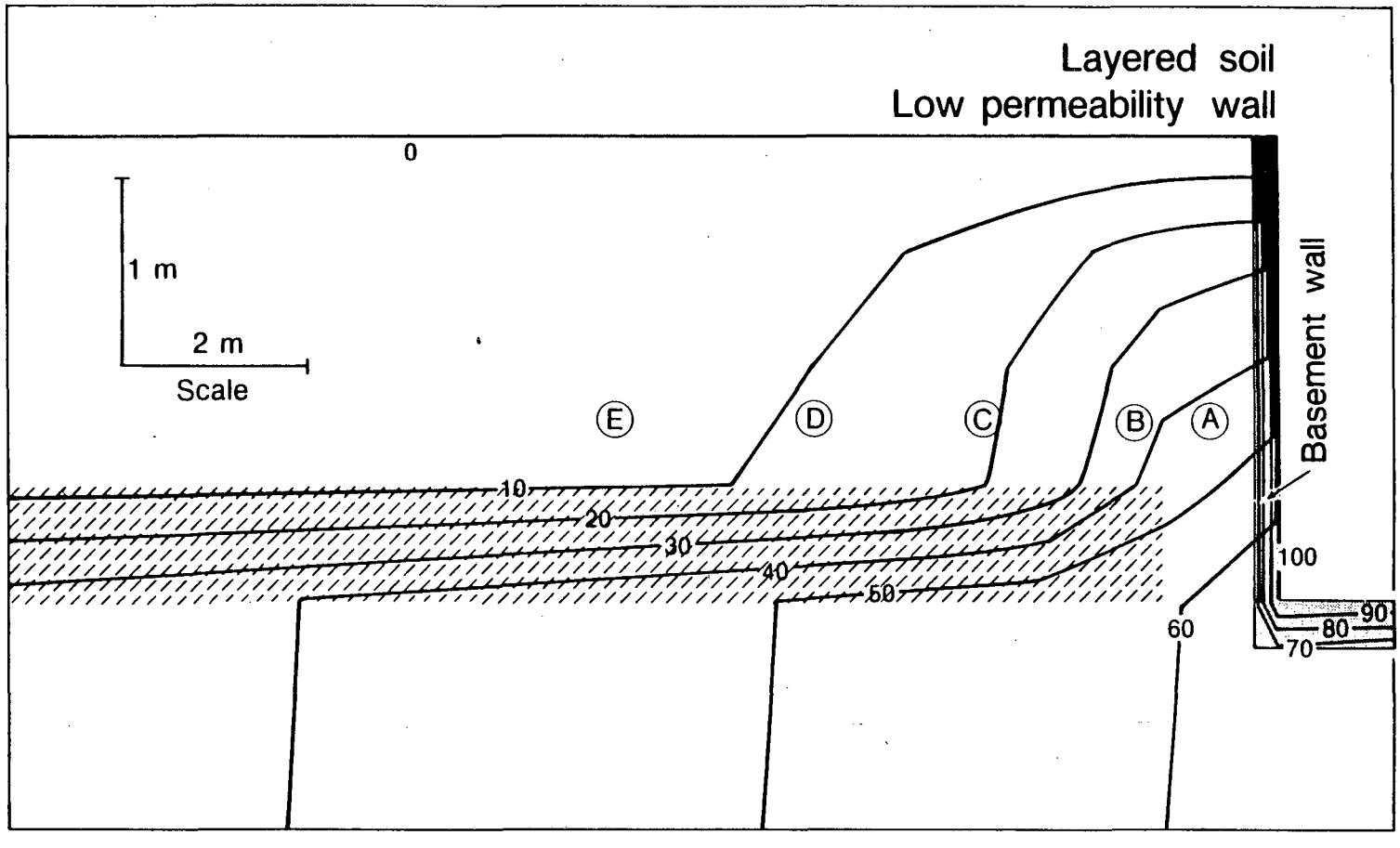

XBL 885-9647

Figure 5.8. Pressure field generated by finite-element model which incorporated a backfill zone in the layered soil and low permeability wall. Pressure contours are percentage of basement underpressure. The zero percent contour is the soil surface. The low permeability soil layer is shaded, and the circles lables (A - E) represent the probe locations.

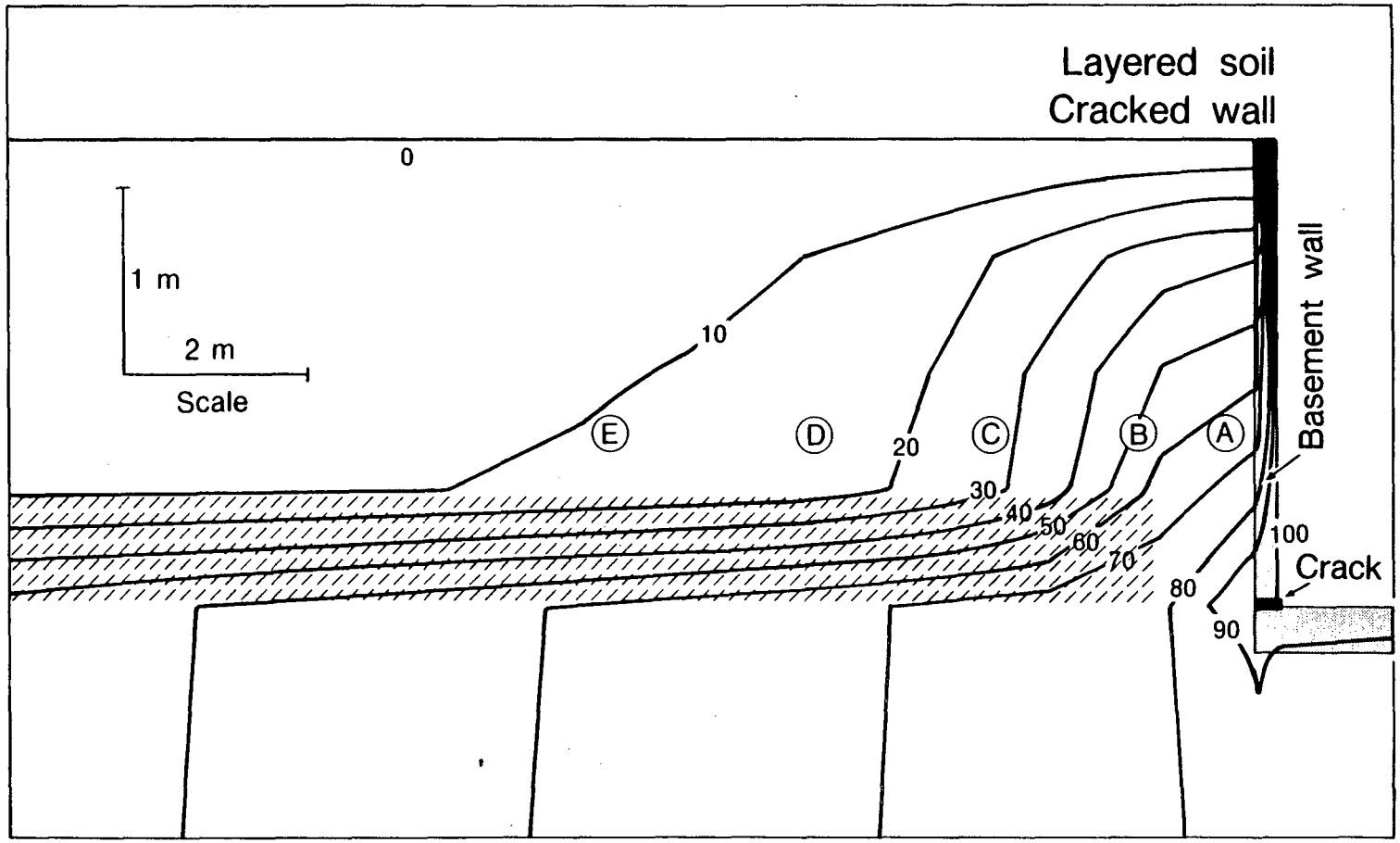

Figure 5.9. Pressure field generated by finite-element model which incorporated a backfill zone in the layered soil and cracked wall geometry. Pressure contours are percentage of basement underpressure. The zero percent contour is the soil surface. The low permeability soil layer is shaded, and the circles lables (A - E) represent the probe locations.

CHAPTER 6

CONCLUSIONS AND RECOMMENDATIONS

Soil and chemical parameters governing the retention and retardation of volatile organic chemicals in soils were investigated by theoretical and laboratory studies. Using the theory of fluid dynamics and empirical expressions for VOC partitioning between air, water, and soil organic carbon, the advection-diffusion equation of the motion of VOC in soil was derived (Equation 2.12). The derivation results in the definition of a retardation factor (Equation 2.11) which determines the contaminant velocity with respect to the velocity of the bulk soil gas. The theoretical retardation factor was compared with experimental data obtained using the soil column apparatus.

A soil-column apparatus and procedure was designed to for three purposes: 1) to test potential tracer-gases for use in field investigations of advective flow of soil gas; 2) for the direct observation of pressure driven transport of VOC through soil; and 3) for screening VOC important as landfill gas contaminants for advective mobility. The pressure-driven transport of two potential tracers, sulfur hexafluoride and hexafluorobenzene, were examined using the apparatus. SF_6 had no measurable retardation or retention in soil, whereas HFB was retarded with respect to SF_6 in all experiments, particularly those conducted in air-dry soil. A retardation factor of approximately 3 was measured for HFB in wetted Panoche soil, in agreement with the theoretical value. The transport experiments using SF_6 and HFB indicate that, under temperature controlled conditions, the soil column apparatus and procedure would be suitable for studying the advective mobility of other VOC. The lack of interaction of SF_6 with soil makes it a suitable tracer for studying the motion of soil gas. The retention of HFB by soil suggests that this compound might mimic the behavior of some VOC important as environmental contaminants, and therefore be a good tracer for studying the long distance transport of sobbing VOC. However a sorbing tracer can pose experimental difficulties in that mass loss to soil can rapidly reduce tracer concentrations in soil gas to undetectable levels, and

retardation of mass flow can result in an unacceptably long residence times.

In the field study concentrations of VOC measured in soil gas, indoor air, and outdoor air indicate that a number of halogenated and oxygenated compound found in indoor air had a soil gas source. Most important among these compounds were dichlorodifluoromethane (Freon-12), trichlorofluoromethane, and tetrachloroethylene. Tracer gas experiments were used to estimate the soil gas entry rate, found to be ~0.1 m^3hr^{-1} under winter heating season (high advective flow) conditions, representing only about 0.1 percent of total house infiltration. Using Freon-12 as an example, the advective entry of VOC from soil gas was compared with estimated diffusive entry. The calculation suggests that, at this house, neither advection nor diffusion dominates soil gas contaminant entry, but rather that both mechanisms contribute.

The field study established, by direct measurement, that pressure-driven flow of soil-gas can result in transport of VOC into houses. In the field house, however, at basement under-pressures characteristic of normal house operation, VOC entry could be explained by either pressure-driven inflow or by diffusion. In houses with a more permeable basement-soil membrane, and with comparably large pressure-coupling, such as those studied by Turk *et al.* (1987), VOC entry via pressure-driven flow could be much larger and result in significantly higher indoor concentrations.

The modified groundwater model proved to be a useful tool for determining the effect of soil layering and basement leakage geometry on the pressure field and for exploring plausible mechanisms to explain the observed pressure coupling. This two-dimension finite element model's flexibility in the designation of different permeabilities for the flow-net elements is a great advantage over previous models. The present model predicted considerably higher coupling than the previous models in both the near and the far-field, providing better agreement with the field data. The pressure-field predicted by the present model was found to be considerably more sensitive to soil geometry than to the leakage geometry of the basement, with near-house pressure coupling more sensitive to model modifications than far-

field coupling. The inclusion of a low-permeability soil layer was found to have a large effect on the predicted pressure field, the net effect being a reduction of near-surface pressure coupling and an increase in coupling with depth and distance from the house. The presence of a soil layer, therefore, can increase the zone of influence of the house, determining the extent of the reservoir from which contaminated soil gas might be drawn.

Recommendations

Although soil heterogeneity and lack of information about soil macro-structure will always introduce uncertainty in predictions of transport of VOC, predictions can be improved by reducing the uncertainty of VOC sorption behavior. If the air-solid sorption rate of VOC were known to be rapid, then, given the sorption coefficient and soil conditions, the simple equilibrium transport model (Equation 2.14) could be used to predict advective flow. The model predictions could then be tested using the soil column apparatus. It is, therefore, recommended that the air-solid sorption kinetics of this class of compounds be further studied. It is further recommended that adsorption isotherms of VOC be conducted to test the data regression (Equation 2.8) for calculation of the soil-sorption coefficient from VOC solubility. Soil-sorption coefficients could then be simply calculated, with less uncertainty than at present and with readily available data. With this information, and with geological data on landfill sites, data on methane pressures in landfills, and landfill gas composition, the number of residences potentially affected by contaminated landfill gas can be estimated. The results of field studies on the uptake of soil gas by houses can then be applied to estimate population exposures to VOC due to gas-phase migration from landfills.

REFERENCES

Bear, J. *Dynamics of Fluids in Porous Media*, American Elsevier Inc., New York, New York, 1972, pp. 125.

Bennet, G.F., "Air quality aspects of hazardous waste landfills," In: *Third International Symposium on Operating European Hazardous Waste Management Facilities*, Odense, Denmark, September 16 - 19, 1986.

Brooks, B.I., and P.J. Young, "The development of sampling and gas chromatography-mass spectrometry analytical procedures to identify and determine the minor organic components of landfill gas," *Talanta* 30(9): 665 - 676 (1983).

California Heath and Safety Code, Section 41805.5 (1986).

CWMB, "A comprehensive plan for management of nonhazardous waste in California," California Waste Management Board, Sacramento, California, 1985.

Chiou, C.T., L.J. Peters, and V.H. Freed, "A physical concept of soil-water equilibria for nonionic organic compounds," *Science* 206(16): 831 - 832 (1979).

Chiou, C.T. and T.D. Shoup, "Soil sorption of organic vapors and effects of humidity on sorptive mechanism and capacity," *Environ. Sci. Technol.* 19(12): 1196 - 1200 (1985).

Chiou, C.T., D.E. Kile, and R.L. Malcolm, "Sorption of vapors of some organic liquids on soil humic acid and its relation to partitioning of organic compounds in soil organic matter," *Environ. Sci. Technol.* 22(3) 298 - 303 (1988).

Day, P.R., "Paricle fractionation and particle-size analysis," In: *Methods of Soil Analysis, Part I*, C.A. Black, D.D. Evans, J.L. White, L.E. Ensminger, F.E. Clarck, and R.C. Dinauer, Eds., American Society of Agronomy, Wisconsin, Chapt. 43, 1965.

DMSA Atcon Ltd., "Review of existing informaton and evaluation for possibilities of research and development of instrumentation to determine future levels of radon at a proposed building site," Report INFO-0096, Atomic Energy Control Board, Ottawa, Canada (1983).

Eichler, D.L., J.H. Mackey, S.F. Niblock, and A.F. Weston, "Entry and dissipation rates of VOCs for residences with basements," For: The 79th Annual Meeting of the Air Pollution Control Association, Minneapolis, Minnesota, 1986.

Hillel, D., *Fundamentals of Soil Physics*, Academic Press, Inc., New York, New York, 1980.

Hodgson, A.T., J. Binenboym, and J.R. Girman, "A multisorbent sampler for volatile organic compounds in indoor air," Paper No. 86-37.1, *Proceedings of the 79th Annual Meeting of the Air Pollution Control Association*, Minneapolis, MN, June 22-27, 1986, Air Pollution Control Association, Pittsburgh, PA (1986).

Hodgson, A.T. and J.R. Girman, "Application of a multisorbent sampling technique for investigations of volatile organic compounds in buildings," In: *Proceedings, ASTM Symposium on Design and Protocol for Monitoring Indoor Air Quality*, April 26-29, 1987, Cincinnati, OH, (In Press).

Hodgson, A.T., K. Garbesi, R.G. Sextro, J.M. Daisey, "Transport of volatile organic compounds from soil into a residential basement," Accepted for presentation to the Air Pollution Control Association Conference, APCA, June, 1988.

Horvath, A.L. *Physical Properties of Inorganic Compounds SI Units*, Edward Arnold Ltd., London, England, 1975.

Karickhoff, S.W., D. Brown, and T. Scott, "Sorption of hydrophobic pollutants on natural sediments," *Water Research* 13: 241 - 248 (1979).

Karickhoff, S.W., "Organic pollution sorption in aquatic systems," *J. of Hydraulic Engineering* 110(6): 707 - 735 (1984).

Klinkenberg, L.J., "The permeability of porous media to liquids and gases," In: *Am. Petrol. Inst. Drilling and Production Practice*, pp. 200 - 213 (1941).

Loureiro, C.O., "Simulation of the steady-state transport of radon from soil into houses with basements under constant negative pressure," (Ph.D. Thesis) Report No. LBL-24378, Lawrence Berkeley Laboratory, Berkeley, CA (1987).

Lyman, W.J., F.R. Reehl, and D.H. Rosenblatt, *Handbook of Chemical Property Estimation Methods: Environmental Behavior of Organic Compounds*, McGraw Hill, New York, New York, 1982.

Mackay D. and W.Y. Shiu, "A critical review of henry's law constants for chemical of environmental interest," *J. Phys. Chem. Ref. Data* 10(4): 1175 - 1199 (1981).

Morse, P.M., and H. Feshbach, *Methods of Theoretical Physics, Part II*, McGraw-Hill Book Co., Inc., New York, New York, 1953, pg. 1300.

Mowris, R.J., "Analytical and numerical models for estimating the effect of exhaust ventilation on radon entry in houses with basements or crawl spaces," (M.S. Thesis) Report No. LBL-22067, Lawrence Berkeley Laboratory, Berkeley, CA (1986).

Nazaroff, W.W., H. Feustal, A.V. Nero, K.L. Revzan, D.T. Grimsrud, M.A. Essling and R.E. Toohey, "Radon transport into a detached one-story house with a basement," *Atmos. Enviro.* 19(1): 31 - 46 (1985).

Nazaroff, W.W., B.A. Moed, R.G. Sextro, K.L. Revzan and A.V. Nero, "Factors influencing soil as a source of indoor radon: A framework for geographically, assessing radon source potentials," Report No. LBL-20645, Lawrence Berkeley Laboratory, Berkeley, CA (1986).

Nazaroff, W.W., S.R. Lewis, S.M. Doyle, B.A. Moed and A.V. Nero, "Experiments on pollutant transport from soil into residential basements by pressure-driven airflow," *Environ. Sci. Technol.* 21(5): 459 - 466 (1987).

Nazaroff, W.W., B.A. Moed and R.G. Sextro, "Soil as a source of indoor radon: Generation, Migration and Entry," In: *Radon and Its Decay Products Indoors*, W.W. Nazaroff and A.V. Nero, Eds., John Wiley & Sons, New York, 1988, pp. 57 - 112.

Nelson, D.W. and L.E. Sommers, "Total Carbon, Organic Carbon, and Organic Matter," In: *Methods of Soil Analysis, Part 2*, A.L. Page, R.H. Miller, and D.R. Keeney, Eds., American Society of Agronomy, Madison, Wisconsin, 539 - 577, 1982.

Nero, A.V. and W.W. Nazaroff, "Characterising the source of radon indoors," *Radon Protection Dosimetry*, 7(1-4): 23 - 39 (1984).

Reeve, R.C. and R.H. Brooks, "Equipment for subsampling and packing fragmented soil samples for air and water permeability tests," In: *Soil Science Soc. Am. Proc.* 333 - 336 (1953).

Roy, W.R. and R.A. Griffin, "Vapor-phase movement of organic solvents in the unsaturated zone, " Open file report prepared for the Environmental Institute for Waste Management Studies at the Unviersity of Alabama, Illinois State Geological, Champaign, Illinois, May, 1987.

Scheidegger, A.E., *The Physics of Flow Through Porous Media*, 3rd Ed., Univ. of Toronto Press, Toronto, 1974.

Sextro, R.G., B.A. Moed, W.W. Nazaroff, K.L. Revzan and A.V. Nero, "Investigations of soil as a source of indoor radon," In: *Radon and Its Decay Products: Occurrences, Properties, and Health Effects*, P. Hopke, Ed., American Chemical Society, Washington D.C, 1987, pp. 10 - 29.

Sherman, M.H. and D.T. Grimsrud, "Measurement of infiltration using fan depressurization and weather data," In: *Proceedings of the 1st Symposium of the Air Infiltration Center on Instrumentation and Measurement Techniques*, Windsor, England, October 6-8, 1980.

Sitar, N., A program for finite element seepage analysis, IBM PC version, Department of Civil Engineering, Unviversity of California, Berkeley, California, Oct. 1985.

Turk, B.H., R.J. Prill, W.J. Fisk, D.T. Grimsrud, B.A. Moed and R.G. Sextro, "Radon and remedial action in Spokane River Valley homes, Volume 1: Experimental design and data analysis," Report No. LBL-23430, Lawrence Berkeley Laboratory, Berkeley, CA (1987).

Wood, J.A. and M.L. Porter, "Hazardous pollutants in class II landfills," *J. Air Pollution Control Assoc.* 37(5): 609 - 615 (1987).

Wu, S. and P.M. Gschwend, "Sorption kinetics of hydrophobic organic compounds to natural sediments and soils," *Environ. Sci. Technol.* 20(7): 717 - 725 (1986).

LAWRENCE BERKELEY LABORATORY
TECHNICAL INFORMATION DEPARTMENT
UNIVERSITY OF CALIFORNIA
BERKELEY, CALIFORNIA 94720